Neutron studies of vibrations in fullerenes

1996 Rep. Prog. Phys. 59 473

(http://iopscience.iop.org/0034-4885/59/4/001)

Rep. Prog. Phys. **59** (1996) 473–510. Printed in the UK

Neutron studies of vibrations in fullerenes

L Pintschovius

Forschungszentrum Karlsruhe GmbH–Technik und Umwelt, Institut für Nukleare Festkörperphysik, Postfach 3640, D-76021 Karlsruhe, Germany

Abstract

Fullerenes are a remarkable new family of carbon phases in which the carbon atoms form closed cages weakly bounded to each other by van der Waals forces. Unique information about the motions of the molecules as a whole as well as about the atomic on-cage vibrations is obtained from inelastic neutron scattering experiments. The results are interesting both on their own for what they tell us about the binding properties of these compounds and, more generally, for the fact that fullerenes are prototypical examples of molecular solids. In particular, solid C_{60} has extremely interesting properties as the molecules are more nearly spherical than in any other molecular solid.

In the first section of this review, the structure of the most important members of the fullerene family is described. Then, an introduction is given into the field of vibrational properties and the experimental techniques used in this field are briefly presented. This is followed by a detailed discussion of the experimental results and their implications for our understanding of the intramolecular and intermolecular binding forces.

This review was received in June 1995

0034-4885/96/040473+38$59.50

Contents

1. Introduction

Although the existence of fullerene molecules was already proven by the pioneering work of Kroto *et al* (1985), investigations of the solid state properties of fullerenes could start only after Kratschmer and co-workers (1990) found a way to mass-produce C_{60} and higher fullerenes. Even then fullerenes became available only in rather small quantities which greatly hampered inelastic neutron scattering studies of the vibrational properties. The neutron scattering technique had to be stretched to its very limits to get meaningful results. Sample purity was another problem, in particular, because of the high sensitivity of inelastic neutron scattering to contamination by hydrogen: as hydrogen has outstanding neutron scattering properties the total mass content of hydrogen had to be brought below 0.1% to reduce unwanted scattering contributions to acceptable levels.

As a consequence of the experimental difficulties just mentioned, the very first investigations of a particular compound yielded often only preliminary results. They were soon outdated when progress in sample preparation made it possible to perform measurements on larger and better characterized samples. Meanwhile, a wealth of reliable information is available which has greatly contributed to our understanding of the solid state properties of fullerenes. In particular, we now have a firm basis to check theoretical concepts for inter- as well as intramolecular binding forces. In respect to the intramolecular binding forces, *ab initio* theory is now able to reproduce the experimental results very closely. On the other hand, the relatively weak intermolecular binding forces are less well understood. Surprisingly enough, even phenomenological potentials which were found to work pretty well for a variety of organic compounds give only a poor account of the orientational potential of C_{60}. A variety of proposals has been made to remedy this situation (Lu *et al* 1992, Sprik *et al* 1992, Yu *et al* 1993, Pintschovius *et al* 1993, Burgos *et al* 1993) but none of the intermolecular potentials proposed so far is able to describe the structure and dynamics of C_{60} in a consistently satisfactory way.

The report is organized as follows. Section 2 summarizes our knowledge on the structural properties of those fullerenes which were investigated by inelastic neutron scattering. Section 3 explains the concepts used in discussions of the vibrational properties of the fullerenes. Section 4 gives a brief introduction into the inelastic neutron scattering technique and describes the major types of instruments. The following four sections will review the experimental results for the four classes of fullerenes investigated so far and will explain how far our understanding of the physical properties has been advanced by the neutron studies. Some concluding remarks will be given in the last section.

2. The structure of fullerenes

Fullerenes form molecular solids in which the molecules are weakly bounded to each other by van der Waals (vdW) forces. Before addressing the crystal structures of the fullerenes we want to describe the structure of the molecules.

The C_{60} molecule has the shape of a truncated icosahedron with 12 pentagonal and 20 hexagonal faces (figure l(*a*), Liu *et al* 1991, Hedberg *et al* 1991, Bürgi *et al* 1992). The diameter of the molecule is $d = 7.1$ Å. There are long bonds (between a hexagon and a pentagon, $l = 1.446$ Å) and short bonds (between two hexagons, $l = 1.402$ Å).

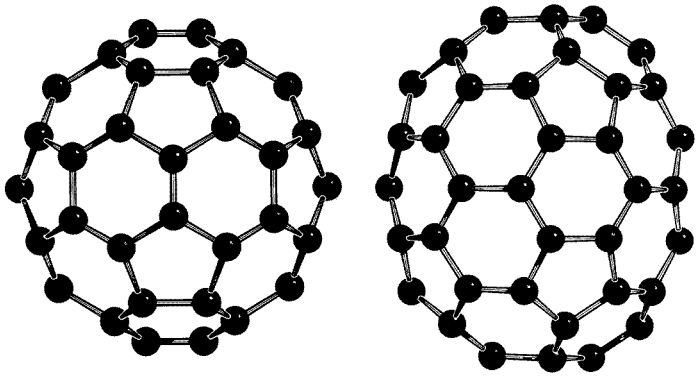

Figure 1. View of the C_{60} molecule (left) and the C_{70} molecule (right). (Reprinted from author's property.)

Long and short bonds are often called single and double bonds, respectively, although the long bonds are considerably shorter than true single bonds ($l = 1.54$ Å) and the short bonds are considerably longer than true double bonds ($l = 1.34$ Å). It appears that, within experimental error, the bond lengths are the same in the gas phase and in the solid state, which is not surprising in view of the weakness of the intermolecular interactions. However, when C_{60} is intercalated with alkali metals or alkali earth metals, the bond lengths do change, as the metal atoms transfer charge to the C_{60} molecules: with increasing charge transfer the bond length alternation is more and more reduced and becomes vanishingly small for C_{60}^{6-} (Andreoni 1993).

Whereas the C_{60} molecule is spheroidal, the C_{70} molecule is markedly elongated along a five-fold molecular rotation axis (see figure l(*b*)). Since the symmetry of the C_{70} molecule is lower than that of the C_{60} one there are eight instead of only two classes of bonds with lengths between 1.37 Å and 1.48 Å (Roth and Adelmann 1992). The average bond length for bonds between a pentagon and a hexagon or between two hexagons is very close to the corresponding values found in C_{60}, i.e. 1.45 Å and 1.42 Å, respectively.

None of the higher fullerenes C_x with $x > 70$ has as yet been investigated by neutrons, the available quantities were simply too small. Therefore we will not deal with their structure here.

A large variety of fullerene derivatives have been prepared by attaching atoms or atom groups to the fullerene molecules. Only a few of these derivatives are of special interest to the solid state physicist. The two derivatives which have so far been investigated by inelastic neutron scattering will be briefly discussed in section 8.

C_{60} crystallizes in a face-centred-cubic (fcc) lattice. The icosahedral molecular symmetry can be made compatible with the local symmetry of the fcc structure only by assuming orientational disorder. Diffraction measurements performed at room temperature indicate that the orientational disorder is nearly maximal, as the data can be very well described by approximating the C_{60} molecule by a hollow sphere (Heiney *et al* 1991). High-quality diffraction data revealed that the C_{60} molecules do show some preferred orientation, albeit to a very moderate extent (Chow *et al* 1992, Schiebel *et al* 1995). From quasi-elastic neutron scattering studies it was concluded that the molecules show rapid reorientational motions (Neumann *et al* 1992, Pintschovius *et al* 1995a, b)—a topic which will be dealt with in section 5.1.1.

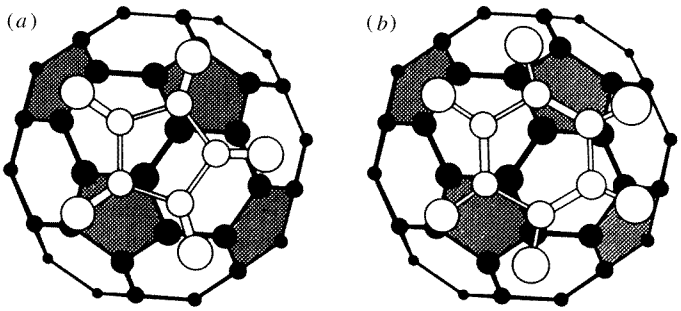

Figure 2. Two views along an axis joining centres of nearest-neighbour C_{60} molecules. In (*a*) the relative orientation is such that a pentagon on the nearer molecule faces a double-bond on the more distant molecule. In (*b*) a hexagon faces the double bond on the more distant molecule. (Reprinted from Copley J R D *et al* 1992 *J. Phys. Chem. Solid* **53** 1353, figure 5. Courtesy of Pergamon Press Ltd.)

On cooling C_{60} below room temperature an fcc-to-simple cubic (sc) phase transition is observed at T 260 K (Heiney *et al* 1991). The phase transition is of first order and involves a slight contraction of the crystal lattice ($a_0 = 14.15$ Å $\rightarrow 14.11$ Å). The molecules remain on fcc sites but assume distinct equilibrium orientations. The low-temperature structure has Pa3 symmetry and contains four molecules in the unit cell. Starting from the standard orientation where the twofold molecular axes are aligned along the cubic [100], [010] and [001] directions, each of the four molecules is rotated about different [111] directions by the same angle Φ. The ground-state orientation is reached for $\Phi \approx 100^\circ$ (we note that some authors use a different convention for defining Φ that leads to $\phi \approx 40^\circ$ for the ground-state orientation). In this case the intermolecular contacts are such that double bonds of one molecule face neighbouring pentagons (David *et al* 1992, see figure 2(*a*)). Accidentally, there is a second orientation which is energetically nearly as favourable as the ground-state orientation: it is reached by increasing ϕ to about 160° and brings double bonds into contact with neighbouring hexagons (David *et al* 1992, see figure 2(*b*)). The near-degeneracy of the two orientations entails a significant amount of orientational disorder: at $T = 250$ K and 90 K about 40% and 18% of the molecules are not in the ground-state orientation, respectively. Some disorder persists even to very low temperatures as the reorientational kinetics becomes extremely slow below the so-called glass temperature $T_g \approx 85$ K (David *et al* 1992, for a review see Meingast and Gugenberger 1993).

When C_{60} is intercalated with the alkali (A) metals potassium or rubidium the A atoms first fill the octahedral sites to form A_1C_{60} and then both the octahedral and the tetrahedral sites to form A_3C_{60} (see figure 3(*a*)). The compounds A_3C_{60} have attracted considerable interest because of their high superconducting transition temperatures (K_3C_{60}: $T_c = 19$ K (Hebard *et al* 1991); Rb_3C_{60}: $T_c = 29$ K (Rosseinsky *et al* 1991)) and therefore were extensively investigated by neutron scattering. Details of the A_3C_{60} structure will be discussed in the context of the vibrational properties in section 6.2.

Solid C_{60} can take up more than three A atoms per molecule to form A_4C_{60} and finally A_6C_{60}. A_4C_{60} is difficult to obtain as a pure phase, whereas A_6C_{60} is much more readily prepared. In contrast to A_3C_{60}, A_6C_{60} is not superconducting and not even metallic. Therefore, it served as a counterpart to superconducting A_3C_{60} in investigations of the vibrational properties. Its structure is displayed in figure 3(*b*).

Instead of Rb or K other alkali metal or earth alkali metal atoms can be filled into C_{60}.

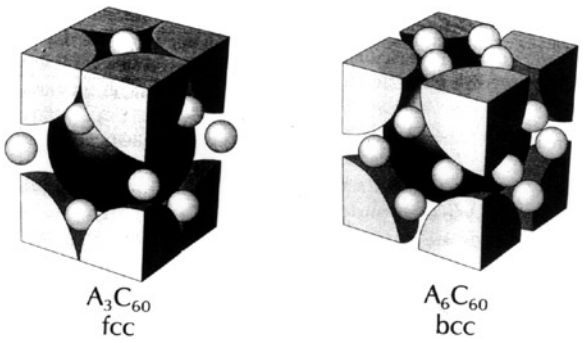

Figure 3. Schematic structures of A_3C_{60} and A_6C_{60} with C_{60} molecules as large spheres and A atoms as the smaller spheres. In A_3C_{60} and A_6C_{60} the C_{60} molecules occupy face-centred cubic and body-centred cubic lattice sites, respectively (from Zhou and Cox 1993). (Reprinted from Murphy D W *et al* 1993 *The Fullerenes* ed H W Kroto *et al* p 151, figure 1 (parts of). Courtesy of Pergamon Press Ltd.)

The structure of these compounds depends much on the radii of the metal ions. For instance, an octahedral site of the C_{60} lattice can accommodate more than one Na ion, so that Na does not form a stable Na_3C_{60} phase. If, however, the octahedral sites are occupied by Rb ions, just one Na atom will fit into the remaining tetrahedral sites to form Na_2RbC_{60}. This compound, too, was investigated by inelastic neutron scattering (Reznik *et al* 1994, see section 6.2).

The crystal structure of C_{70} is still less well understood than that of C_{60}. As-grown crystals show either a fcc or a hexagonal close-packed (hcp) structure at room temperature (Van Tendeloo *et al* 1993). This indicates that the two structures are extremely close in free energy. This is corroborated by the observation of a high density of stacking faults in C_{70} crystals.

Since the high local symmetry of the fcc or hcp lattice is inconsistent with the symmetry of the 'rugby-ball shaped' C_{70} molecule, the molecules have to be assumed to be orientationally disordered. To what extent the disorder is static or dynamic is not precisely known. In section 7.3 we will review investigations where this question was addressed by quasi-elastic neutron scattering.

Several first-order phase transitions have been observed in the temperature range 250 K to 360 K (van Tendeloo *et al* 1993, Meingast *et al* 1994). Details of these phase transitions are still unclear. Qualitatively it can be said that these phase transitions involve a successive freezing-out of rotational degrees of freedom. At low temperatures the structure of C_{70} can be viewed as a deformed hep structure in which the long axis of the molecules is aligned along the hexagonal c-axis. Orientational ordering gives rise to a superstructure leading to a monoclinic unit cell containing two molecules rotated by 180° with respect to each other (Van Tendeloo *et al* 1993).

3. Vibrational properties: general concepts

Since in solid fullerenes the intermolecular forces are much weaker than the intramolecular forces, the vibrations can be very well classed into two distinct groups: *external* and *internal* vibrations. External vibrations involve the fullerene molecule as a whole, which can be considered as an essentially rigid body. The external vibrations involve either translational

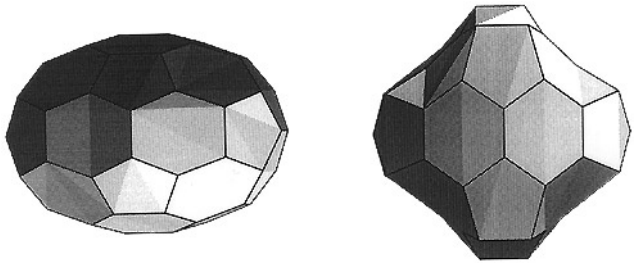

Figure 4. Schematic representation of the displacement pattern of the two lowest H_g modes of the C_{60} cage. Left: $H_g^{(1)}$, right: $H_g^{(2)}$ (from Heid *et al* 1995).

or rotational motion of the molecules and are sometimes labelled accordingly as translations and vibrations. The latter name refers only to motions where the rotation is hindered, i.e. the motion of the molecules is oscillatory. It does not apply to jump-like or nearly free reorientational motions as are observed in solid fullerenes at elevated temperatures.

The internal vibrations involve changes of the bond distances or bond angles of the carbon atoms on the fullerene molecule. A fullerene molecule C_x has $3(X-2)$ types of internal vibrations. These vibrations can be classed into several groups according to the symmetry of the displacement patterns. For instance, the internal vibrations of C_{60} molecules are classified as follows:

$$2A_g + A_u + 3T_{1g} + 4T_{1u} + 4T_{2g} + 5T_{2u} + 6G_g + 6G_u + 8H_g + 7H_u\,.$$

From these, four are infrared active (T_{1u}) and ten are Raman active (A_g, H_g), whereas the remaining 32 modes are optically inactive ('silent') so that they can be explored only by inelastic neutron scattering. The total number of modes (46) is much lower than $3 \times (60-2) = 174$ as the T-modes are triply, the G-modes fourfold and the H-modes fivefold degenerate. These degeneracies are a consequence of the high symmetry of the C_{60} molecule.

A different classification of the internal vibrations is based on the observation that some modes involve primarily carbon atom displacements in the radial direction and others in the tangential one. The energies of radial modes and tangential modes are determined by bond angle bending and bond stretching stiffnesses, respectively. Therefore, typical radial modes and typical tangential modes are found at the lower and at the higher end of the spectrum, respectively. Examples for displacement patterns are depicted in figure 4. We note that these displacement patterns are not determined by symmetry alone, but depend also on the intramolecular force constants. Therefore, a complete characterization of the vibrations requires not only a determination of the mode frequencies, but also of the mode eigenvectors.

When the fullerene molecules are packed into a crystal lattice, the internal vibrations are slightly altered: degeneracies are lifted and the energy of the modes depends on the phonon wavevector, i.e. the modes show dispersion. However, as the intramolecular forces are so much stronger than the intermolecular forces these changes are rather small. This is illustrated in figure 5 which shows the phonon dispersion of C_{60} as calculated from a phenomenological model fitted to a variety of experimental data (Yu *et al* 1993). It can be seen that the vibrational modes of an isolated C_{60} molecule evolve into bands less than 2 meV wide. For modes with $E > 100$ meV the band width is practically negligible.

Figure 5 is very illustrative not only for showing the influence of the crystal lattice on the internal vibrations but also for giving realistic mode frequencies: external vibrations

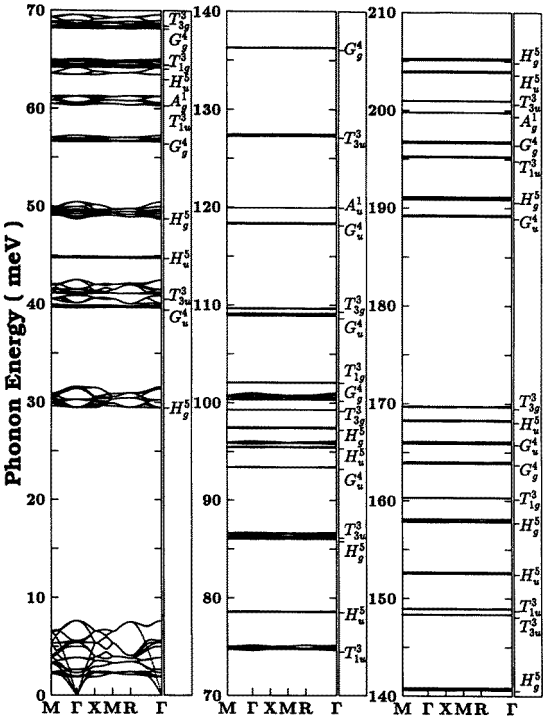

Figure 5. Calculated phonon dispersion curves of solid C_{60} along high-symmetry directions. The vibrational frequencies of an isolated C_{60} molecule are given by the bars on the right-hand side of the diagram and are labelled according to the symmetry of the molecule (from Yu *et al* 1993). (Reprinted from Yu *et al* 1993 *Appl. Phys. Lett.* **63** 3152, figure 1. Courtesy of the American Institute of Physics.)

have energies well below 10 meV, so that they are separated by a large energy gap from the internal vibrations (which is the very basis for a clear distinction between the two groups). The energy range of the internal vibrations is very large and extends to about 200 meV, which is far beyond the range of vibrational energies of ordinary metals or ionic solids.

Intercalation of C_{60} with alkaline metals gives rise to additional vibrational modes. To a good approximation the metal atoms behave like Einstein oscillators with energies in the range of or slightly above the energies of the external vibrations.

4. Inelastic neutron scattering techniques

In inelastic neutron scattering experiments neutrons with incident energy E_0 and wavevector $\boldsymbol{k}_0$ are scattered by the sample to have the final energy E_1 and wavevector $\boldsymbol{k}_1$ (where $\overline{h}k = \sqrt{E/2m_n}$ with m_n being the neutron mass). Maxima of the scattered intensity are observed for scattering processes involving the creation or annihilation of one phonon with energy $\overline{h}\omega$ and wavevector $\boldsymbol{q}$ ($\boldsymbol{q}$ lies in the direction of the phonon propagation and $q = 2\Pi/\lambda$ is the wavelength of the phonon). The energy and wavevector of the excited (de-excited) phonon follows from the conservation equations

$$\overline{h}\omega = E_0 - E_1 \tag{1}$$

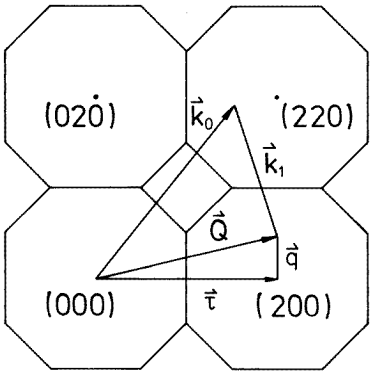

Figure 6. Representation of an inelastic neutron scattering diagram in reciprocal space. The example shown refers to a measurement in the (001) scattering plane of an fcc lattice. (Reprinted from author's property.)

$$\boldsymbol{k}_0 - \boldsymbol{k}_1 = \boldsymbol{Q} \tag{2}$$

and

$$\boldsymbol{Q} = \boldsymbol{\tau} \pm \boldsymbol{q} \tag{3}$$

where $\boldsymbol{Q}$ is the total momentum transfer and $\boldsymbol{\tau}$ is a reciprocal lattice vector. Equations (2) and (3) are visualized in figure 6. Equation (3) applies only to coherent scatterers (which is the case for the fullerenes) which form a regular lattice (which is the case for most although not all fullerene samples). Using equations (1)–(3) the energy versus wavevector relation $\omega = \omega_j(\boldsymbol{q})$ is obtained, where $j = 1, \ldots, 3N$ is the branch index and N the number of atoms in the unit cell. Information on the displacement patterns of the $3N$ phonon branches is obtained by comparing the scattering intensity for the same $\boldsymbol{q}$, but different $\boldsymbol{\tau}$ values.

If the sample is investigated in polycrystalline form only a direction-averaged information on the excitation spectrum will be obtained. Often, the results are further averaged over a large range of momentum transfers which yields essentially the phonon density of states (PDOS). As has been discussed in the previous section the dispersion of the branches associated with the internal vibrations of the fullerene molecules is small so that the PDOS seems largely sufficient to characterize the internal vibrations. On the other hand, a determination of the PDOS using powder samples does not yield any information on the displacement patterns so that an assignment of the observed excitations has to rely solely on theoretical predictions or by comparison with results of optical experiments.

A variety of neutron spectrometers have been used to study the fullerenes, the choice depending on the range of excitation energies of interest and whether the sample was available as single crystal or only in polycrystalline form. Many measurements were performed on a standard triple-axis spectrometer (figure 7(*a*)). Here, the neutrons emanating from the core of a research reactor are monochromatized by a Bragg reflection at a monochromator crystal and then impinge on the sample. Only those scattered neutrons that are Bragg reflected by an analyser crystal reach the detector. Collimators σ_i narrow down the neutron flight path to ensure well defined values of the neutron energies E_i and E_f and wavevectors $\boldsymbol{k}_0$ and $\boldsymbol{k}_1$. This type of instrument is designed for studies of the phonon dispersion relations on single crystals, but can be used for powder samples as well, although the efficiency for measurements on powders is usually inferior to that of time-of-flight (TOF) instruments described below. Triple-axis spectrometers were sometimes chosen for the simple reason of being readily accessible.

So far the available single crystals of fullerenes were too small to be investigated on standard triple-axis spectrometers. Therefore, all the single crystal studies were performed

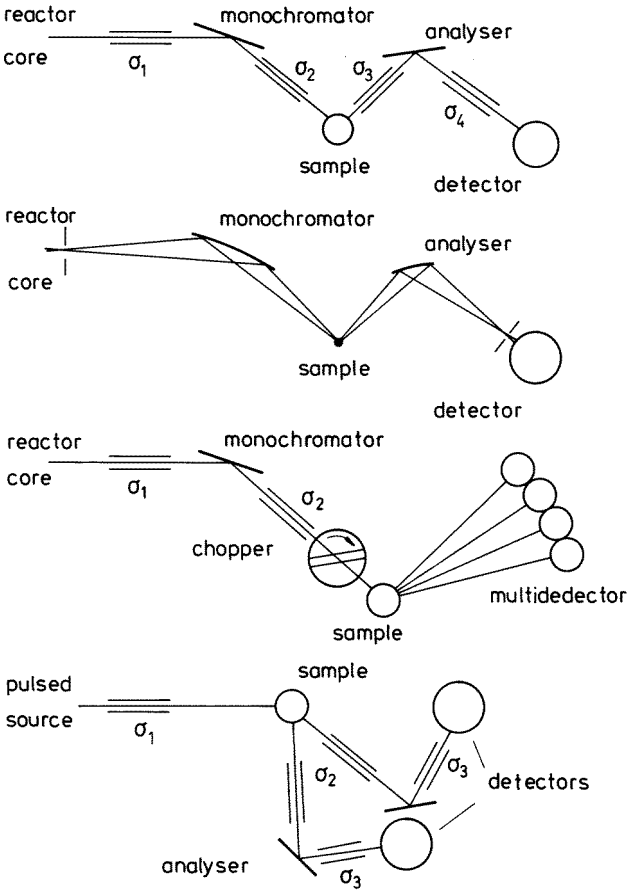

Figure 7. Schematic representation of different types of instruments used for inelastic neutron scattering investigations. From top to the bottom. (*a*) Conventional triple-axis spectrometer. (*b*) Triple-axis spectrometer for very small samples using focusing monochromator and analyser crystals. (*c*) Reactor-based time-of-flight spectrometer. (*d*) Pulsed-source-based time-of-flight spectrometer using the so-called inverted geometry. (Reprinted from author's property.)

on a special instrument (Pintschovius 1994) using focusing Bragg optics (figure 7(*b*)). Even on this instrument the minimum sample volume is $\sim$2 mm^3 which could be achieved only for undoped C_{60}. Furthermore, as the scattering cross section decreases substantially with increasing energy transfer, all the early measurements had to be restricted to the energy range of the external vibrations. It was only very recently that single crystals of C_{60} with volume $\sim$0.1 mm^3 became available which allow one to study also the internal modes. First results obtained by Heid *et al* (1995) will be presented in section 5.2.

Polycrystalline samples are usually studied on TOF instruments. When the instrument is located at a reactor the neutron beam is first monochromatized, then chopped into short pulses ($\sim$30 μs), scattered by the sample and finally detected in one of the many detectors surrounding the sample (figure 7(*c*)). The energy of the scattered neutrons is computed from the TOF between the opening of the chopper and the arrival at the detector. The advantage of such an instrument is that scattered neutrons are registered over a rather large solid angle.

Reactor-based instruments have a serious shortcoming for studies of fullerenes: the useful range of neutron energies extends only to ∼130 meV, and therefore only excitations with energies less than ∼100 meV can be studied in a satisfactory way, whereas the spectrum of the internal vibrations in fullerenes goes far beyond that. For very high energy transfers instruments located at pulsed sources (so-called spallation sources) clearly outperform reactor-based instruments. An instrument especially designed for large energy transfers is represented in figure 7(*d*): the polychromatic ('white') beam impinges on the sample and the scattered neutrons reach the detector after being Bragg reflected by one of the analyser crystals. The incident neutron energy is computed from the TOF between the pulse generated in the source and the arrival at the detector; the final neutron energy is given by the Bragg angle at the analyser crystal. The characteristics of the neutron source (i.e. the pulsewidth versus neutron energy relation) is such that a good energy resolution is maintained up to very high energy transfers. Also for medium energy transfers (20 to 100 meV) the energy resolution is superior to that of a standard reactor-based instrument. The drawback of such a machine is that geometrical constraints do not allow one to install a large number of detectors making it relatively demanding in respect to the sample mass. Therefore, the available quantities of fullerenes did not allow one to fully exploit the capabilities of the instrument.

5. Phonons in solid C_{60}

As has been explained in section 3, the vibrations of solid C_{60} can be classified into external and internal vibrations, and experimental investigations of these two types will yield information on the intermolcular and intramolecular forces, respectively. We start with a discussion of the external vibrations. As the intermolecular forces will sensitively depend on the relative orientations of the molecules, the external vibrations in the ordered and in the disordered phase are discussed separately.

5.1. External vibrations

5.1.1. Dynamics in the disordered phase. NMR measurements (Tycko *et al* 1991) provided the first evidence that the orientational disorder in the high temperature phase of C_{60} ($T > T_s \sim 260$ K) is dynamic. Quasi-elastic neutron scattering was used to determine the time scale and the detailed nature of the reorientations.

The first results were obtained on powder samples by Neumann *et al* (1991) and Renker *et al* (1993). A strong quasi-elastic signal was observed for $T > T_s$ whose intensity and linewidth was strongly modulated as a function of momentum transfer Q (figure 8). The observed scattering could be well described by a model in which each molecule undergoes rotational diffusion which is uncorrelated with the motion of adjacent molecules (see the full curves in figure 8). Solid C_{60} appeared as a prototypical example of a rotator phase in which the reorienting molecules are more nearly spherical than in any other molecular solid exhibiting similar behaviour. One of the results of Neumann *et al* (1991), however, did not fully fit into the remarkably simple picture of the rotational dynamics: the diffusion constant D_R was found to be lower than expected for freely rotating molecules and the temperature dependence of D_R was consistent with a thermally activated process having an activation energy of 35 ± 15 meV. Obviously, there is a sizeable rotational barrier.

Later, quasi-elastic measurements performed on single crystals (Pintschovius *et al* 1995a, b) showed that the simple picture of uncorrelated rotational diffusion does not hold. It was found that the quasi-elastic intensity is strongly modulated not only in the radial but

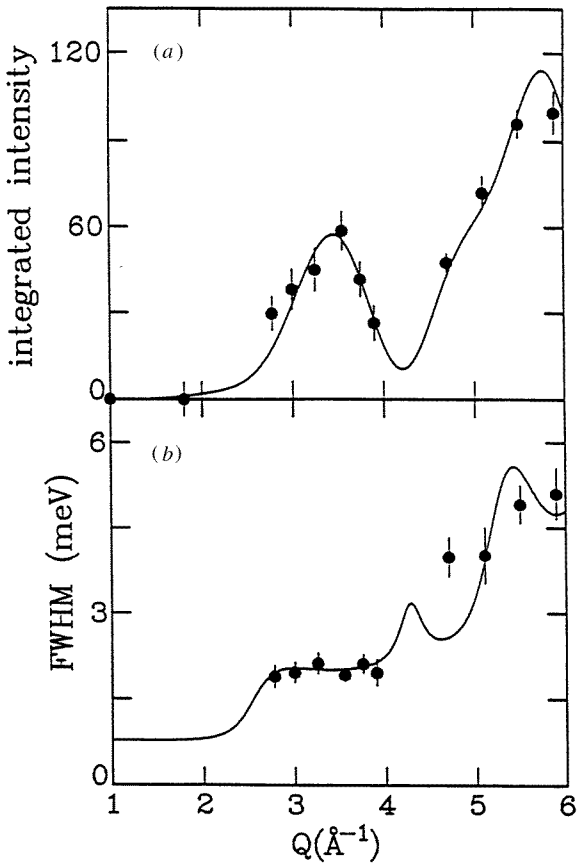

Figure 8. Q dependence of (a) the integrated intensity and (b) the full width at half maximum of the quasi-elastic scattering. The solid lines are the result of a calculation where each molecule undergoes rotational diffusion with no correlation between the motions of adjacent molecules. The rotational diffusion constant was chosen as $D_R = 1.4\times10^{10}$ s^{-1}. (Reprinted from Neumann D A *et al* 1992 *Phys. Rev. Lett.* **67** 3808. Courtesy of the American Institute of Physics.)

also in the tangential direction and that in certain crystallographic directions the modulation is much sharper than expected from a model assuming uncorrelated reorientational motions. So the sharpness of the peaks is direct evidence of intermolecular correlations (see figure 9). At temperatures just above T_s a correlation length l_c was deduced from the width in Q to be $l_c \sim 40$ Å which is four times the shortest intermolecular distance. Energy scans performed at positions of intensity maxima yielded a much smaller linewidth than scans performed at positions of intensity minima (see figure 10). So the diffuse peaks look like pseudo-Bragg peaks and indicate a pronounced degree of local orientational order.

An obvious idea to explain the diffuse peaks is to consider them as a critical phenomenon, i.e. as a precursor effect of the disorder–order transition. What unambigously speaks against this idea, however, is the fact that most of the diffuse peaks are not observed at those positions in reciprocal space where the superlattice Bragg peaks are found in the low temperature phase. This means that the local order in the high-T phase cannot be associated with the appearance of embryos of the low-T phase. We note that critical scattering at the superlattice peak positions has indeed been observed (Blaschko *et al* 1993, Pintschovius *et*

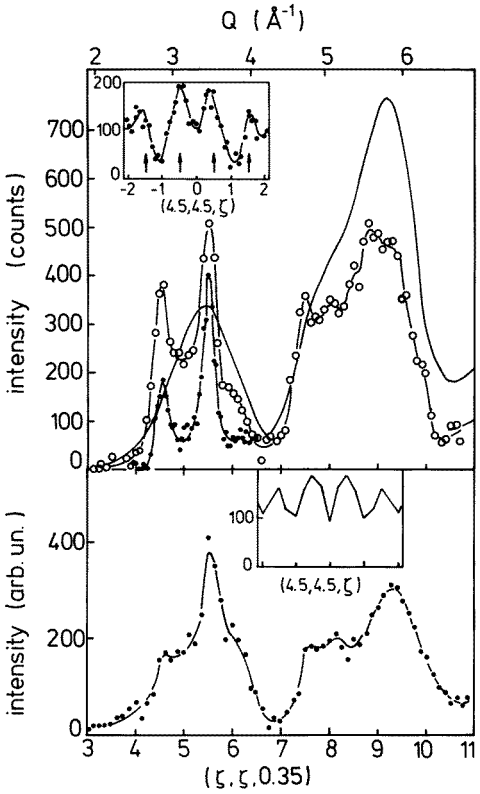

Figure 9. Upper panel: diffuse scattering intensity along the line $(\zeta,\zeta,0.35)$ as observed by neutron scattering. (All indices refer to a cubic lattice with $a_0 = 14.16$ Å). The points refer to measurements using different energy windows (circles: $\Delta E = 2.1$ meV, full points: $\Delta E = 0.7$ meV FWHM). The full line shows the calculated energy integrated intensity distribution for uncorrelated rotational diffusion from Renker *et al* (1993a). Scaling of the three curves is arbitrary. The insert shows a high resolution measurement in the transverse direction. The arrows correspond to 2 a_0 fcc superlattice spot positions. Lower panel: results calculated from a molecular dynamics simulation. (Reprinted from Pintschovius L *et al* 1995c *Phys. Rev. Lett.* **75** 2843.)

al 1995b), but only in a very narrow temperature region (~2 K) above T_s, whereas the local order indicated by the diffuse peaks discussed above persists to much higher temperatures.

The local orientational order is not yet fully understood but what comes out very clearly from the analysis performed so far (Pintschovius *et al* 1995b, c, Chaplot and Pintschovius 1995a) is that the driving force for the local order is the same as that for the long range order below T_s. That is to say the molecules tend to align in such a way that double bonds of one molecule face pentagons or hexagons of adjacent molecules. What makes the diffuse peaks appear at different positions in reciprocal space than the supperlattice spots of the ordered phase is the fact that the local structures are partly frustrated. That is to say a sizeable fraction of the molecules have orientations which correspond to a local minimum of the orientational potential but are incompatible with long range order.

We emphasize that the pronounced local order found by quasi-elastic scattering is not incompatible with only weakly developed preferred orientations concluded from Bragg diffraction data. An analysis of diffraction data yields a superposition of all the molecular

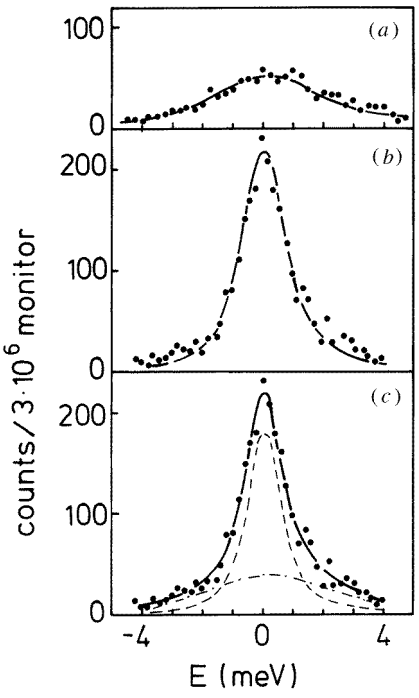

Figure 10. Energy scans performed at positions in reciprocal which correspond to a local minimum ((*a*), $Q = (0.35, 5, 5)$) or a local maximum ((*b*) and (*c*), $Q = (0.35, 5.5, 5.5)$) of the intensity versus Q distribution shown in figure 9. The full curves are the result of a fit using a relaxation ansatz for the scattering law $S(E) = A(1-\exp(-E/kT))E\Gamma/(E^2+\Gamma^2)$ and folding it with the experimental resolution ($\Delta E = 0.7$ meV, FWHM). In (*c*) the full curve was obtained as the sum of a narrow component (broken curve) and of a broad component having the width like in (*a*) (chain curve). (Reprinted from Pintschovius L *et al* 1995c *Phys. Rev. Lett.* **75** 2843.)

orientations on a single site and superposing the different orientations of adjacent molecules will give an average atomic density which is close to that of a uniform hollow sphere.

Now we turn to the translational motions of the molecules involving displacements of the centres of mass. For the neutron studies of these motions only very small single crystals with volume of $V = 2$ to 5 mm^3 were available. As has been mentioned in section 4 a specialized instrument (figure 4(*b*)) had to be used to make measurements on small crystals feasible. In spite of the small sample size rather precise data could be obtained for most of the phonon branches in the main symmetry directions (Pintschovius *et al* 1992, Pintschovius *et al* 1993, Pintschovius and Chaplot 1995).

It was found that the translational motions can be very well described in the phonon picture, i.e. as travelling waves with well defined wavevector $\boldsymbol{q}$ and energy E. The phonon dispersion relation (figure 11) looks very simple and can be very well described by a model where the C_{60} balls are connected with longitudinal springs to each other. Only a very close look reveals that more elaborate models are needed to obtain a perfect reproduction of the data. This might be interpreted as a manifestation of the fact that the C_{60} molecules are not completely spherical and show local orientational order. However, the improvement of the fit quality by more sophisticated models like the one shown in figure 11 (above) brings only the final touches as the simple model is already so good. The only other solids we know of, whose phonons can be described with similarly simple models, are the solid noble gases. As the noble gases crystallize in the same structure (fcc) the phonon dispersion relations can be directly compared to that of C_{60}. As is illustrated by the broken curves in figure 11, the shape of the phonon dispersion curves is extremely similar for both types of solids (by accident, even the energies match very well with those of krypton).

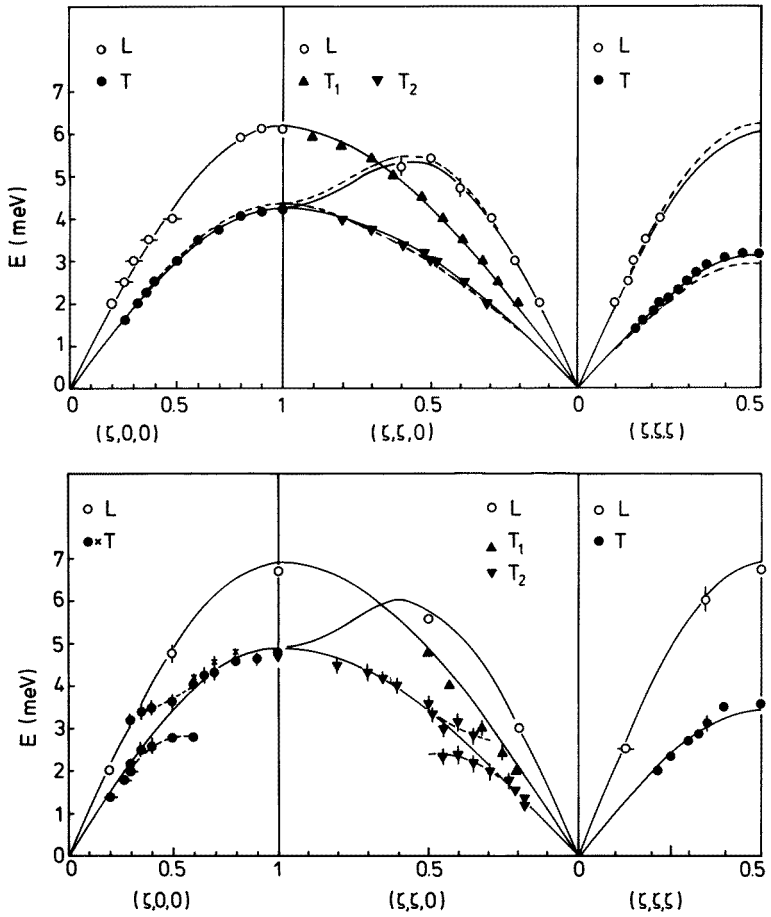

Figure 11. Upper panel: dispersion curves of the translational phonons of solid C_{60} at room temperature. The symbols L and T denote phonons of longitudinal and transverse polarization, respectively. The full curves were calculated from a three-parameter force constant model (from Pintschovius and Chaplot 1995). The broken lines depict the phonon dispersion curves of solid krypton at $T = 10$ K (from Skalyo *et al* 1974). Lower panel: frequencies of phonon modes of C_{60} with predominantly translational character at $T = 200$ K. The data were plotted in an extended zone scheme to emphasize the similarity to the room temperature data. Only those data were compiled in this figure that correspond to modes of the room temperature phase plotted in the upper panel. The full curves were calculated from a one-parameter force constant model. (Reprinted from Pintschovius L and Chaplot S L *Z. Phys.* B, in print, figures 2 and 6 (modified). Courtesy of Springer-Verlag.)

5.1.2. Lattice dynamics in the ordered phase: translations, vibrations and their coupling. The phonon dispersion relations in the ordered phase are of much greater complexity than in the disordered phase: we have now 24 different phonon branches in each direction instead of only 3. Why this large increase? Firstly, the reorientational motions are no longer diffusive, but oscillatory around the equilibrium positions, giving rise to the same number of *librational* phonon branches as the *translational* ones (we note that from a variety of experimental techniques such as NMR there is evidence that large angle reorientational jumps do also occur in the ordered phase, but at such a low rate that the orientations of

the C_{60} molecules can be considered as time-independent on the time scale of the external vibrations). The second reason for the large increase in the number of phonon branches is the fact that the unit cell in the ordered phase contains four molecules instead of only one, so that we have 4×3 translational and 4×3 librational branches.

The phonon dispersion relations predicted by theory are depicted in figure 12 (the lattice dynamical model underlying these predictions will be discussed in some detail in section 5.1.4; we note that these results are not truly predictions as the model parameters were tuned using preliminary experimental data). The dispersion of the translational branches is displayed on figure 12(*a*). The dispersion relations are not so much different from that of the fcc-phase as it might seem in the first instance. We note that the relatively flat optic branches around 4.5 meV and 6.5 meV correspond to fcc-branches of very similar energy which are folded in from the fcc-zone boundary into the first Brillouin zone of the sc-phase. Further, all the branches in the $(\zeta, 0, 0)$- and in the $(\zeta, \zeta, 0)$-direction are folded back at the new zone boundary $(0.5, 0, 0)$ or $(0.5, 0.5, 0)$, respectively. What is really specific to the sc-phase are some moderate splittings like those between the E_u-, A_u- and T_u-modes around 4.6 meV. In addition, small so-called anticrossing gaps appear, as branches of the same symmetry are not allowed to cross each other. In short, the locking-in of the molecular orientations is expected to produce only a minor disturbance of the translational branches.

The librational branches are displayed in figure 12(*b*). Naively one would expect the vibrations to form three bands corresponding to the three librational degrees of freedom per molecule. However, theory predicts that this simple picture is valid only in the T-direction where all the branches are fourfold degenerate. The full phonon dispersion (figure 14 (below)) cannot be obtained by a simple superposition of figures 12(*a*) and 12(*b*), as the translational and the librational degrees of freedom interact with each other creating a large number of anticrossing gaps.

When trying to disentangle the phonon dispersion relations experimentally the first problem confronting the investigator is how to discriminate between phonon peaks associated with translations from those associated with librations. Model calculations revealed that clear selection rules exist only for relatively small Q (i.e. $Q < 3$ Å^{-1}). Here, measurements will yield only translational phonon peaks, albeit with rather low intensity. The determination of librational energies requires measurements at larger Q where, however, the scattering cross sections for translations and librations are comparable. The assignment of the observed peaks has to rely on quantitative predictions of a lattice dynamical model. As lattice dynamical models are notoriously less reliable in respect to intensities than in respect to energies, redundant data are needed for an unambignous assignment.

In some cases it was found that the excitations have neither a clear translational nor a librational but a mixed character. Experimental evidence for such a case is shown in figure 13. This mixing can be understood from the fact that the molecules are tightly engaged in the low temperature phase. As is illustrated at the top of figure 13 such an engagement will result in rotational motions of the molecules when their centres of mass are displaced and vice versa.

An overview on the experimental results is given in figure 14 (above). The main results can be summarized as follows. (i) The phonon dispersion of the translations is similar to that of the fcc-phase, apart from a general hardening of the energies by $\sim$10% (see figure 11 (below)). This hardening can be understood as a consequence of the lattice contraction. (ii) The librations have a relatively high energy. In addition to librations with energies around 2.5 meV which were already known from powder measurements (Copley *et al* 1992) the single crystal studies revealed librations with energies up to 4.5 meV. The conclusions which

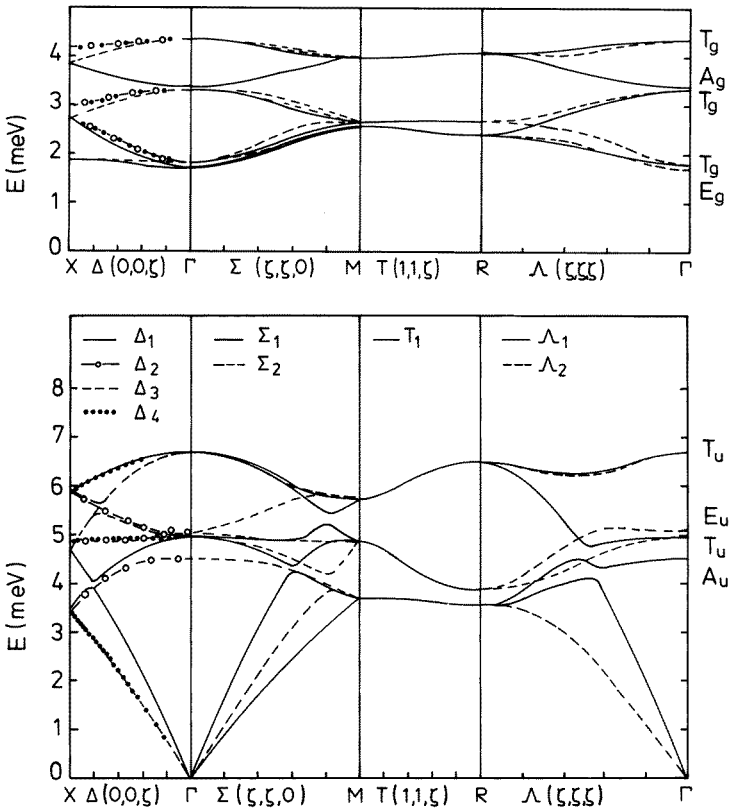

Figure 12. Calculated phonon dispersion curves of the external vibrations in the low temperature phase of C_{60}. The upper and lower panels depict branches of librational and translational character, respectively. The coupling between librational and translational degrees of freedom was deliberately ignored in this calculation. The symmetry of the modes is indicated by different symbols using the group theoretical notation. (Reprinted from Pintschovius L and Chaplot S L 1995a *Z. Phys.* B, **98** 527, figures 7(*a*), (*b*). Courtesy of Springer-Verlag.)

can be drawn from these results regarding the intermolecular potential will be discussed in section 5.1.4.

5.1.3. The order–disorder transition. As has been discussed above, the rotational motion of the C_{60} molecules is diffusive above T_s and oscillatory below T_s. Therefore, the two phases above and below T_s can be called an orientational liquid and an orientational solid, respectively. The fact that a significant amount of short-range orientational order is present in the high-temperature phase does not contradict to call it an orientational liquid, as ordinary liquids show short-range order phenomena as well. Starting from this picture of an orientational liquid/solid the order–disorder transition can be called an orientational freezing transition (respectively an orientational melting transition when viewed from below T_s).

There is ample evidence from a variety of experimental techniques that the transition is of first order. Therefore it cannot be expected that any particular phonon mode will go soft at the phase transition temperature. Indeed, a rather strong general softening of the phonon modes was observed on approaching the phase transition from below, but no real soft mode behaviour (Pintschovius *et al* 1993, Pintschovius and Chaplot 1995). From the temperature

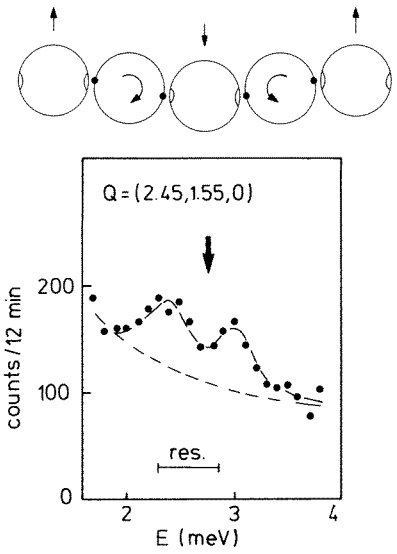

Figure 13. Inelastic neutron scattering scan measured for solid C_{60} in the low temperature phase ($T = 200$ K). In the high temperature phase the corresponding scan shows a single peak at the position denoted by the arrow. This peak is associated with transverse acoustic phonons. The peak splitting observed in the low-temperature phase is due to a coupling between librational and translational degrees of freedom as illustrated schematically in the upper part of the figure. (Reprinted from Pintschovius L and Chaplot S L 1995a *Z. Phys.* B, **98** 527, figures 9 and 10. Courtesy of Springer-Verlag.)

dependence of the lowest librational phonon energy a temperature can be estimated where the molecules will start to rotate rather freely. The extrapolated phase transition temperature is ∼450 K which is nearly 200 K above the actual T_s (Pintschovius and Chaplot 1995a).

Early experimental results obtained on powders were interpreted as evidence for a very strong damping of the librations at temperatures close to T_s with linewidths exceeding the librational energies (Copley *et al* 1992). This would indicate very strong anharmonicity, possibly associated with large amplitude librational motions. However, the single crystal data (Pintschovius *et al* 1992, Pintschovius and Chaplot 1995) do not support this hypothesis: well defined phonon peaks associated with vibrations were observed even very close to T_s, the linewidth remaining moderate (see figure 15). The increase in linewidth at elevated temperatures might be associated not so much with anharmonicity in the classical sense, i.e. with large amplitudes probing a non-quadratic potential, but with an increase of the orientational disorder as mentioned in section 2. As will be discussed in the next section lattice dynamical models based on empirical intermolecular potentials predict a strong effect of orientational disorder on the librational excitations.

5.1.4. Intermolecular potentials: achievements and shortcomings. In view of the large intermolecular carbon-carbon distances $r \geqslant 3$ Å it was obvious to assume that the intermolecular binding forces are of the vdW type. Therefore the intermolecular potential V was modelled either by a Lennard-Jones potential

$$V(\mu, v) = 4\varepsilon \sum_{i,j=1}^{60} \left\{ \left(\frac{\sigma}{(r_{i\mu} - r_{jv})} \right)^{12} - \left(\frac{\sigma}{(r_{i\mu} - r_{jv})} \right)^{6} \right\} \tag{4}$$

with ε and σ as parameters, or by a Buckingham potential, where the repulsive part is assumed to fall off exponentially. The parameters of the potential were taken from organic compounds or from graphite, as it seems very likely that the interlayer binding forces in graphite are the same as the intermolecular binding forces in C_{60}. Indeed, the lattice constant and the cohesive energy of C_{60} were obtained in good agreement with experiment. Also the vibrational properties in the disordered phase were reproduced quite accurately, including the elastic constants and the bulk modulus (Pintschovius and Chaplot 1995). This

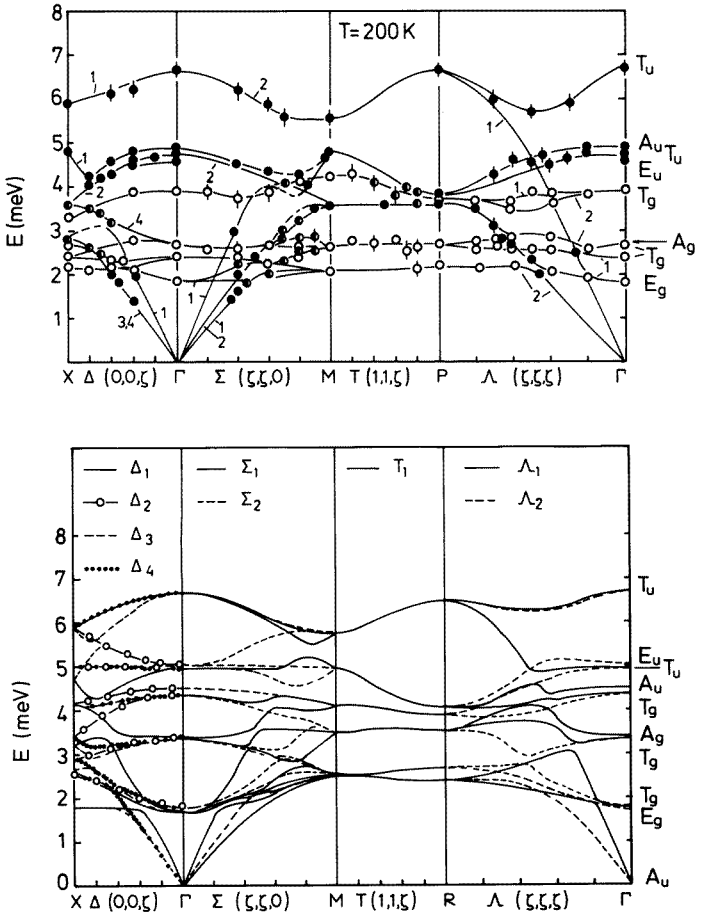

Figure 14. Experimental (above) and theoretical (below) dispersion curves of the external vibrations of solid C_{60} in the low temperature phase. The data were taken at $T = 200$ K. The theoretical curves are based on a split-bond charge model (Pintschovius *et al* 1993) including the coupling between translational and librational degrees of freedom. The notation is the same as in figure 12. (Reprinted from Pintschovius L and Chaplot S L 1995a *Z. Phys.* B, **98** 527, figures 7(*c*) and 8(*c*). Courtesy of Springer-Verlag.)

means that the radial dependence of the intermolecular potential appears to be correct. On the other hand, all properties which follow from the orientational potential show serious discrepancies between theory and experiment. To begin with, the orientational potential shows only a local minimum for the ground-state orientation of the low-temperature phase with an energy ∼100 meV above that of another seemingly more favourable orientation (Guo *et al* 1991, Lu *et al* 1992). In experiment, this second orientation was found to lie ∼12 meV above the ground state orientation (David *et al* 1993). Further, the curvature of the potential—either for the true ground state or for the calculated ground state—is much too small to account for the observed librational frequencies: the corresponding force constants are too low by a factor ∼5 (Pintschovius *et al* 1992). Also the calculated lock-in phase transition temperature is much lower than observed which is another indication that the orientational potential is too soft (Lu *et al* 1992).

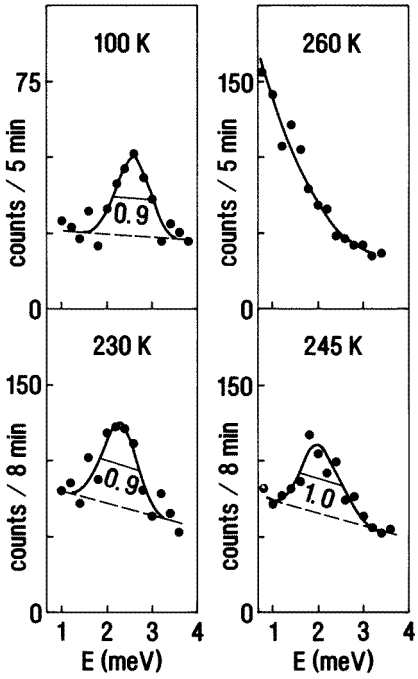

Figure 15. Constant-Q scans taken on solid C_{60} at $Q = (5, 4, 4)$ at different temperatures. The instrumental resolution is about 0.8 meV. (Reprinted from Pintschovius L *et al* 1992 *Phys. Rev. Lett.* **69** 2662, figure 5. Courtesy of the American Institute of Physics.)

Several proposals have been made to remedy the situation. They all consider electrostatic interactions as the basic ingredient to arrive at a better description of the experimental observations. Point charges were put on various places of the molecule: Lu *et al* (1992) and Yu *et al* (1993) put a positive charge q on the single bond and $-2q$ on the double bond; Sprik *et al* (1992) also put a negative charge on the double bond but place the compensating positive charge onto the carbon atoms; the same is done by Pintschovius *et al* (1993), however, with the negative charge on the double bond split in the radial direction; finally Burgos *et al* (1993) place negative charges on the double bonds and positive ones at the centres of pentagons. In all these models the vdW part of the potential is retained, either unchanged or slightly scaled down (Pintschovius *et al* 1993) to compensate the additional binding energy associated with the electrostatic interactions. Sprik *et al* (1992) also included explicitly interaction sites on the double bonds for vdW interactions.

The electrostatic interactions produce two effects: they lower the energy of the true ground-state orientation in respect to the other orientation and they considerably stiffen the orientational potential. This means that the two major deficiencies of the simple Lennard-Jones potential are remedied at the same time. After a proper tuning of the model parameters several static and dynamic properties are calculated in good agreement with experiment. In particular, the split-bond charge model of Pintschovius *et al* (1993) reproduces the dynamic properties very closely (see figures 13 and 14).

Although the empirical intermolecular potentials just mentioned do much better than the simple Lennard-Jones potential, they are probably of limited use for a real understanding of the intermolecular forces in C_{60}. First of all, a calculation of electrostatic multipole moments of C_{60} using the quantum mechanical charge distribution yielded values about 10 times smaller than those predicted from the point charge models (Yildirim *et al* 1993). Therefore it is not surprising that the correct multipole potential, although improving the Lennard-Jones potential to some extent, is by itself too small to stiffen the orientational

potential as much as needed. So something else is needed beyond electrostatic interactions to understand the orientational potential in C_{60}. Unfortunately, theory is not yet capable of predict the orientational potential from *first principles*. *Ab initio* calculations revealed that chemical bonding (hopping) is important for the molecular orientation and the cohesive energy (Gunnarsson *et al* 1991), but too many simplifying assumptions had to be made to extract quantitative results.

In spite of the fact that the point charges used in the empirical potentials look somewhat unphysical one might ask if they, nevertheless, give a realistic parametrization of the intermolecular binding properties. The potentials do reproduce several static and dynamic properties quite satisfactorily, but also have serious shortcomings. For instance, the good description of the vibrational properties by the split-bond charge model mentioned above is obtained under the assumption that all the molecules sit in the ground-state orientation. However, when assuming a realistic degree of orientational disorder theory predicts that all librational phonon peaks should be strongly broadened which is in conflict with the observations (see figure 16). Even stronger disorder effects have been found for another empirical potential (Yu *et al* 1993) and will follow very probably from all the models proposed so far. This indicates that the models, although reproducing the ground-state properties, fail to correctly describe the orientational potential for the whole range of molecular orientations. This suspicion is confirmed when looking at the model predictions for large angular displacements. For instance, figure 17 depicts the potential energy of a C_{60} molecule rotated away from its ground-state orientation around different rotation axes whereby the neighbouring molecules are kept fixed in their ground-state orientation. Figure 17(*a*) was calculated from the potential of Lu *et al* (1992) and figure 17(*b*) depicts the shape of the curves which is needed to be compatible with all the relevant experimental information. The curves of figure 17(*b*), taken from Axe *et al* (1994), were constructed *ad hoc* without any explicit expression for the intermolecular potential. To find such an expression remains a challenge!

5.2. Internal vibrations

5.2.1. Experimental results. In the first experiment reported on neutron spectroscopy of the internal vibrations of C_{60}, that of Capelletti *et al* (1991), the energy transfer range between 26 and 215 meV was examined with a filter-detector spectrometer located at the NIST research reactor. A filter-detector spectrometer is closely related to the triple-axis spectrometer depicted on figure 7(*a*). The only difference is that energy analysis of the diffracted neutrons is not achieved by a Bragg reflection at an analyser crystal but instead by a filter which rejects all but very low-energy neutrons. Two spectrometer configurations were used, one with a relatively low overall resolution (5–18 meV) but permitting the observation of the highest energy modes, and a high-resolution set-up (2–4 meV) for energy transfers 25 meV $\overline{h}\omega < 80$ meV. A highly structured spectrum was observed for $\overline{h}\omega < 120$ meV, the loss of structure at larger energy transfers being probably due to insufficient resolution (see figure 18). The lower part of the figures indicate where vibrational modes had been observed by optical spectroscopy or were expected from theoretical calculations. Obviously, although theory and experiment agree on the energy range of the internal vibrations, assignment of the observed peaks often remains ambiguous, and the assignment problem prevented any rigorous check of the theoretical results.

As has been pointed out in section 4 TOF spectrometers at spallation sources are particularly powerful for high-resolution measurements of high energy vibrations. The first measurements on such a spectrometer were performed by Prassides *et al* (199la). When

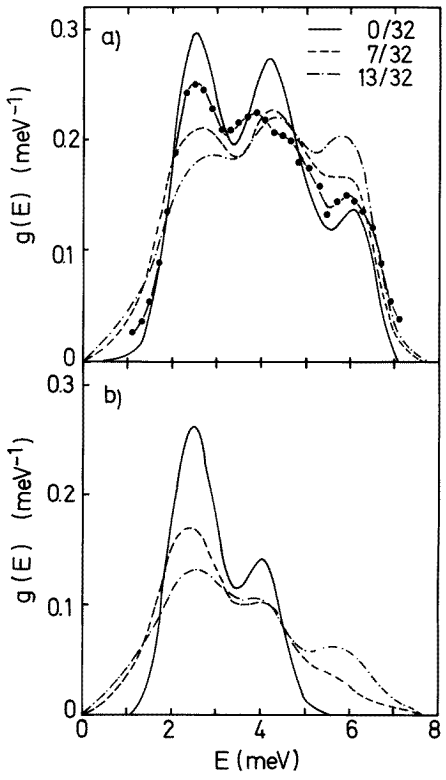

Figure 16. Intermolecular phonon density of states (PDOS) calculated from the split-bond charge model for different amounts of orientational disorder using a 32 molecule supercell, i.e. with 0, 7 and 13 of the molecules being in the minority orientation, respectively. The data points were taken from Gompf *et al* (1994). For the sake of comparison the calculated spectra were folded with the experimental resolution (0.8 meV). Above: full PDOS, below: librational part only. (Reprinted from Pintschovius L and Chaplot S L 1995a *Z. Phys.* B, **98** 527, figure 20. Courtesy of Springer-Verlag.)

larger samples became available Coulombeau *et al* (1992) were able to obtain well resolved spectra up to 200 meV (see figure 19). Later, Coulombeau *et al* (1994) realized that the low energy part of the spectrum suffers from a very high background but the data seem to be reliable for $E > 30$ meV. The energy resolution up to $\hbar\omega \sim 100$ meV is excellent. For larger energy transfers, however, insufficient statistics called for smoothing of the raw data so that the resolution became too poor to resolve individual modes. Further progress was achieved by measurements on another spectrometer (Coulombeau *et al* 1994, see figure 20). From these measurements it is evident that the energy range of the internal vibrations does not extend beyond 200 meV.

Recently, Copley *et al* (1995) reported a high-resolution spectrum for 30 meV $< E <$ 130 meV obtained by the filter-detector method. The peak positions, though not the peak intensities, agree very well with those reported by Coulombeau *et al* (1992).

As mentioned above, assignment of the observed frequencies to individual modes is a non-trivial problem. Optical data are a great help in sorting out infrared active and Raman active modes, but as pointed out in section 3 as many as 32 modes are optically inactive. Model calculations have shown (Heid *et al* 1995) that a great deal of information on the character of the modes could be gained even from powder samples when systematic measurements of the peak intensities are made as a function of the momentum transfer. The filter-detector spectrometer of Capelletti *et al* (1991) or Copley *et al* (1995) is unfit for this purpose, but the TOF spectrometer used in the study of Coulombeau *et al* (1994) would be appropriate provided very large samples or very long counting times are available. Measurements on single crystals using a triple-axis spectrometer would allow one to exploit not only the Q- but also the direction dependence of the scattering intensity and therefore

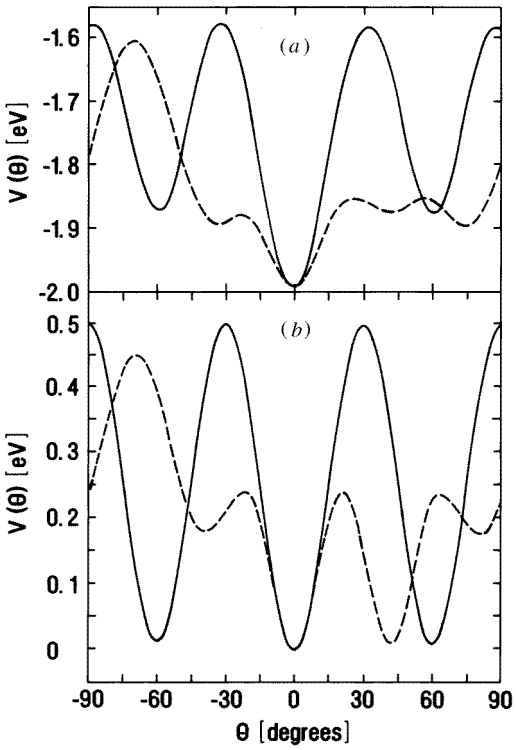

Figure 17. Schematic diagram of the single particle orientational potential in the low temperature phase of C_{60}. Here $\Theta = 0$ corresponds to the equilibrium position of the C_{60} molecule, the solid lines represent the potential for rotations of the molecule about the three-fold axis aligned along a $\langle 111 \rangle$ direction, and the broken curve is the potential for rotations about the $\langle 1-10 \rangle$ direction which nearly corresponds to a twofold axis of the molecule. The minority orientation can be reached by a 60° rotation about $\langle 111 \rangle$ or a ~42° rotation about $\langle 1-10 \rangle$. Above: calculated for the bond charge model of Lu *et al* (1992). Below: curves sketched by Axe *et al* (1994) as to be compatible with a large body of experimental information. (Reprinted from (*a*) Lu J P *et al* 1992 *Phys. Rev. Lett.* **68** 1551. Courtesy of the American Institute of Physics.) (*b*) Axe J D *et al* 1994 *Solid State Phys.* **48** ed M Ehrenreich and F Spaepen p 149, figures 22 (redrawn). Courtesy of Academic Press.

Heid *et al* (1995) embarked on this task. A first result is shown in figure 21: the 50 meV phonon is now unambiguously assigned to the $H_u^{(1)}$-mode.

5.2.2. Intramolecular binding forces from theory. Whereas for the *inter*molecular interactions only empirical potentials are available, the *intra*molecular forces were successfully studied by *first-principles* methods, too. In a *first-principles* study of the vibrational modes the first step is to calculate the electronic wavefunction of the C_{60} molecule using the density-functional approach within the local density approximation (LDA). Starting from a trial geometry of the molecule the geometry is optimized with respect to the total energy of all the electrons in the system. The calculated geometry of the molecule was always found to be in very good agreement with that derived from experiments. In the next step of the calculation the molecule is distorted and the intramolecular force-constants are obtained via a calculation of the forces exerted on all the atoms in the molecule arising from the distortion.

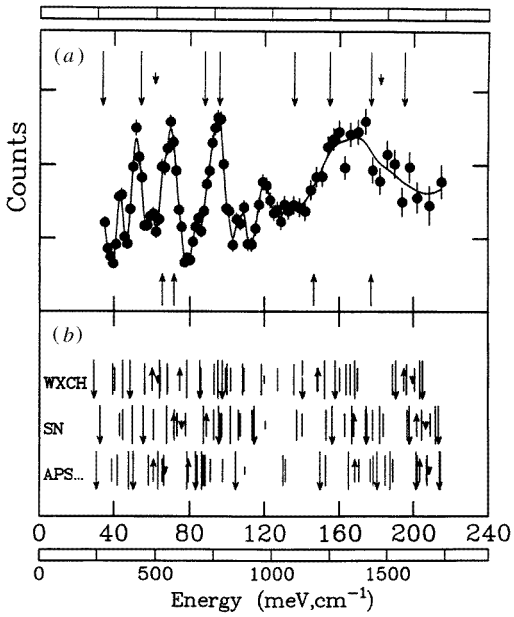

Figure 18. (*a*) Vibrational spectrum for C_{60} measured on a filter-detector spectrometer at the NIST research reactor (Cappelletti *et al* 1991). The ordinate is proportional to the phonon density of states of the external vibrations, except that a smooth background is present, which rises at higher energies. Upward- and downward-pointing arrows represent observed infrared-active and Raman active modes (Bethune *et al* 1991). The length of the arrows is proportional to mode degeneracies. (*b*) Calculated frequencies from Wang *et al* (1991), Stanton and Newton (1988) and Adams *et al* (1991). The arrows and their lengths have the same meaning as in (*a*). The figure was taken from Cappelletti *et al* (1991). (Reprinted from Cappelletti R L *et al* 1991 *Phys. Rev. Lett.* **66** 3261, figure 1. Courtesy of the American Institute of Physics.)

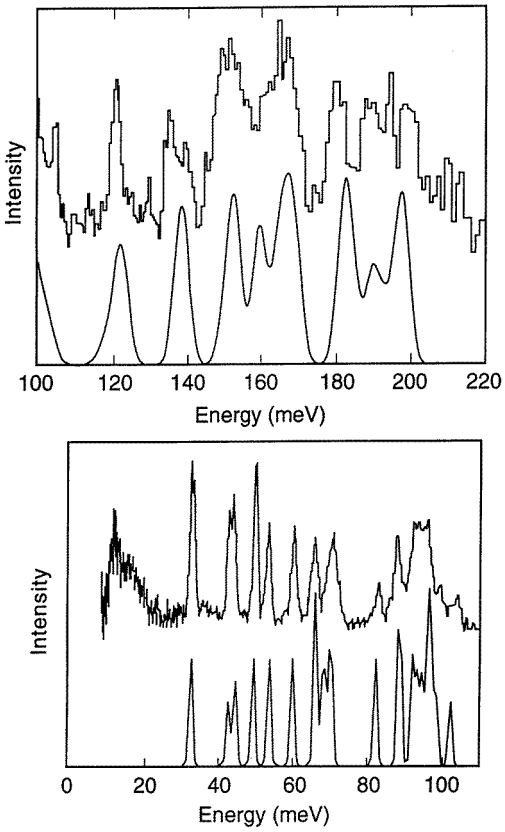

Figure 19. Upper panel: comparison between the experimental neutron inelastic scattering spectra (top) of Coulombeau *et al* (1992) and the vibrational density of states of the C_{60} molecule (bottom) as calculated on the basis of a first-principles theory by Wang *et al* (1993) for the energy range 100–220 meV. The theoretical results were broadened by a Gaussian function with a standard deviation of 1.9 meV. Lower panel: the same as in the upper panel, but for the low frequency modes. The broadening of the theoretical results was done with a Gaussian function with a standard deviation of 0.5 meV. The figure was taken from Wang *et al* (1993). (Reprinted from Wang X Q *et al* 1993 *Phys. Rev.* B **48** 1884, figures 1 and 2. Courtesy of the American Institute of Physics.)

Various computational schemes have been proposed involving the displacement of a

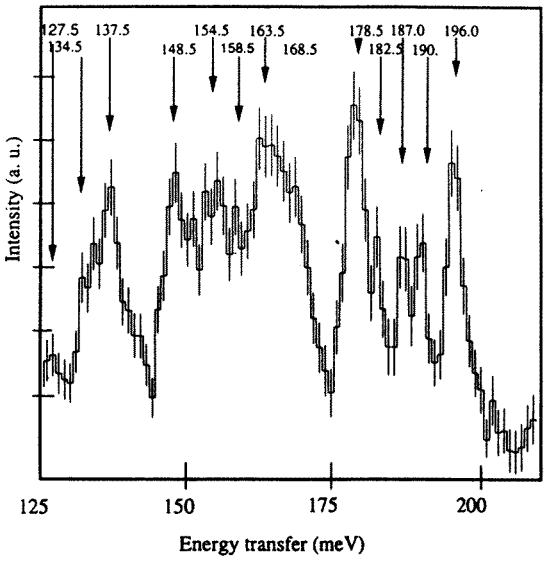

Figure 20. Experimental spectrum of the high frequency modes of C_{60} measured with very good resolution by Coulombeau *et al* (1994). (Reprinted from Coulombeau C *et al* 1994 *Full. Sci. Technol.* **2** 247, figure 4. Courtesy of Marcel Dekker, Inc.)

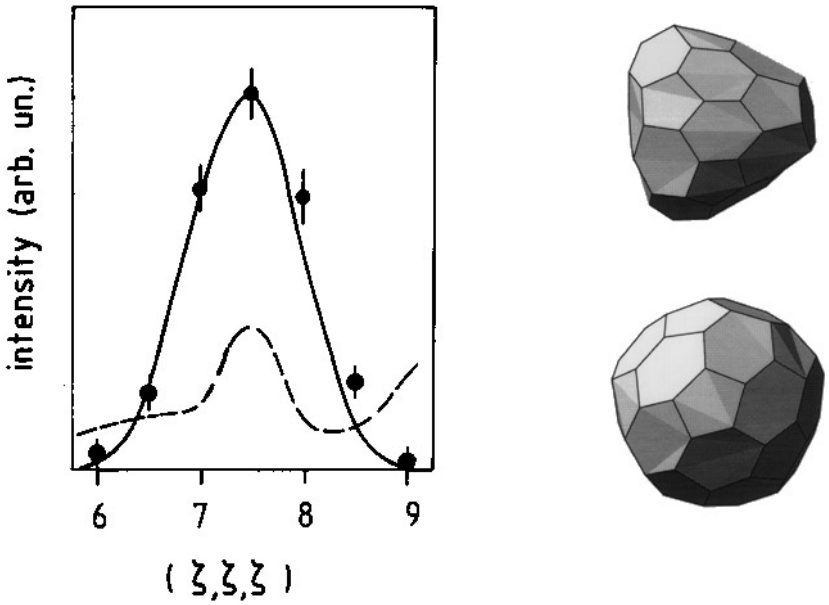

Figure 21. Intensities of the 50 meV peaks observed in solid C_{60} at $T = 12$ K along the $\langle 111 \rangle$ direction. The lines were calculated using the displacement patterns of the $H_u^{(1)}$-mode (full curve) or the $G_u^{(1)}$-mode (broken curve). The relative scaling of the data to the calculated curves was based on more data than those shown here. The displacement patterns of the two modes are shown on the right-hand side of the figure (above: $H_u^{(1)}$, below: $G_u^{(1)}$) We note that different theories suggest different assignments because of somewhat different calculated energies. For instance, the force constant model of Jishi *et al* (1992) predicts the energies of the $H_u^{(1)}$ and $G_u^{(1)}$ modes at $E = 45.1$ meV and 48.2 meV, respectively, whereas the *ab initio* result of Wang *et al* 1993 is $E = 49.1$ meV and 44.1 meV. (After Heid *et al* 1995, property of the author.)

single atom (Jones *et al* 1992, Faulhaber *et al* 1993, Wang *et al* 1993), two atoms on

opposite sides (Bohnen *et al* 1995), all atoms displaced in a highly symmetric way (Bohnen *et al* 1995) or all atoms displaced in an arbitrary manner (Adams *et al* 1991, Feuston *et al* 1991). Displacement of all atoms in arbitrary directions has the disadvantage that the calculation cannot profit from the high symmetry of the molecule, and therefore it is not surprising that the results obtained in this way are less precise than those obtained by the other methods (this method was developed to study finite temperature properties. In the case of C_{60}, however, this bears only for very high temperatures, i.e. 1000 K or more).

The vibrational properties are usally computed for isolated molecules. When the molecules were put into a crystal lattice a non-realistic crystal symmetry was used, i.e. fcc, to avoid the computational complexity associated with having four molecules in the unit cell as deduced from experiment (Bohnen *et al* 1995). This means that calculation of the lattice effects on the internal modes is beyond the scope of present-day *ab initio* theory.

As can be seen from figure 19 the calculated vibrational frequencies of Wang *et al* (1993) compare extremely well with those obtained by inelastic neutron scattering. We note that the recent results of Coulombeau *et al* (1994) fully support the theoretical predictions for the very high energy vibrations (see figures 19 and 20). In as far as the symmetry of the modes is known from optical experiments it is found that theory predicts the correct symmetry of the individual modes. The assignment of the silent modes at energies 40 meV $< E <$ 50 meV achieved recently by Heid *et al* (1995) fully supports the *ab initio* results.

With the *first-principles* theory being very successful, is there any room for empirical or semiempirical theories? One might think that empirical theories with adjustable parameters may outperform *first-principles* calculations in respect to accuracy. Indeed, the Raman-active and infrared-active modes of C_{60} were reproduced on the basis of force-constant models quite accurately (Jishi *et al* 1992, Onida and Benedek 1992). However, the other modes not included in the fitting database were reproduced with much less accuracy (see, e.g. figure 21) so that on the whole the empirical models are not superior in accuracy to the best *first-principles* calculations. What remains a real advantage of the empirical potentials is the fact that they can be used to study the lattice effects on the internal vibrations, i.e. to calculate the dispersion of these vibrations. The results of such a calculation were already shown in a previous section (figure 5).

6. Vibrations in doped C_{60}

Both the external and the internal vibrations of doped C_{60} have been studied by several groups. The motivation was twofold: firstly, to understand the modification of the inter- and intramolecular force field arising from intercalation of C_{60} with alkaline metal atoms, and secondly, to search for signatures of a strong electron–phonon coupling and thereby to contribute to the understanding of the relatively high superconducting transition temperatures found in this class of compounds. These two aspects will be addressed in what follows.

6.1. Intermolecular and dopant vibrations

When alkaline atoms are intercalated into the C_{60} lattice, the intermolecular distances are slightly expanded which entails a softening of the intermolecular vibrations. On the other hand, the filling of the interstitial sites by alkaline atoms leads to an increased rotational hindrance potential and also stiffens the translational motions to some extent. The resultant effect is that the translational frequencies change very little, whereas the librational frequencies are markedly higher than in pure C_{60} (Renker *et al* 1992b, see figure 22).

The hardening of the librational frequencies is least pronounced in Na_2RbC_{60} (Christides

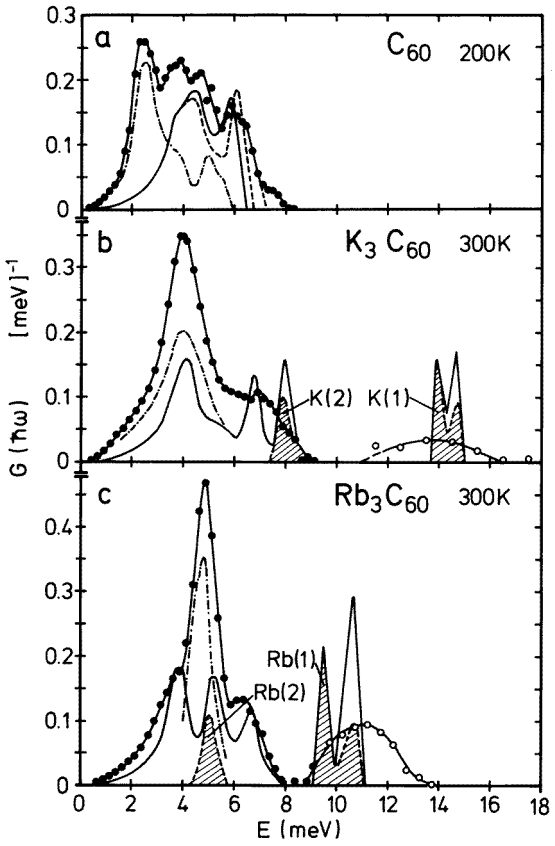

Figure 22. The neutron cross section weighted PDOS of low-frequency modes in pure (*a*) C_{60}, (*b*) K_3C_{60} and (*c*) Rb_3C_{60}. The experimental spectra were normalized to unity. Contributions from the metal atom vibrations measured in energy gain are shown by open circles. The various curves were obtained via lattice dynamical calculations aiming at a decomposition of the total spectra into contributions from translational C_{60} phonons (thin full and broken curves), librational C_{60} phonons (chain curves) and alkali atom vibrations (shaded areas). A(1) and A(2) atoms are occupying the tetrahedral and octahedral voids, respectively. (Reprinted from Renker B *et al* 1993b *Z. Phys.* B **92** 451, figure 4. Courtesy of Springer-Verlag.)

et al 1993, see figure 23). Here, the big Rb atoms occupy the octahedral sites, whereas the smaller tetrahedral sites are filled by the relatively small Na atoms. If, however, the big Rb atoms are also squeezed into the tetrahedral sites, the librational frequencies increase by about 70%. This increase is not quite as large when all the sites are filled by K atoms because of the smaller ionic radius (figure 23). Very high librational energies ($\sim$6 meV) were observed in Rb_6C_{60} which is probably due to the greater number of Rb atoms surrounding a C_{60} molecule (Christides *et al* 1992).

The vibrations of the alkaline atoms appear to lie at the upper end of the spectrum of the intermolecular vibrations (Renker *et al* 1993b, see figure 22). The energies of the motions of the alkaline atoms occupying the tetrahedral sites are considerably higher than those of the atoms sitting in the octahedral sites. We note that the latter energies are difficult to determine experimentally because of the overlap with the intermolecular vibrations. The analysis of the experimental spectra shown in figure 22 was based on a fit under very simplifying assumptions. In particular, the same A–C_{60} force constants were used for A = K and A = Rb. This led presumably to an overestimate of the energies of the K vibrations. From a structure analysis it is known that the octahedral site is so large that the K(2) atom shows a very large temperature factor, which indicates static or dynamic disorder, resulting in displacement of the K(2) atom away from the centre of the octahedral site (Rosseinsky 1994). Therefore, it has to be expected that the K(2) vibrations are quite low in energy, i.e. considerably lower than 8 meV as is assumed in figure 22.

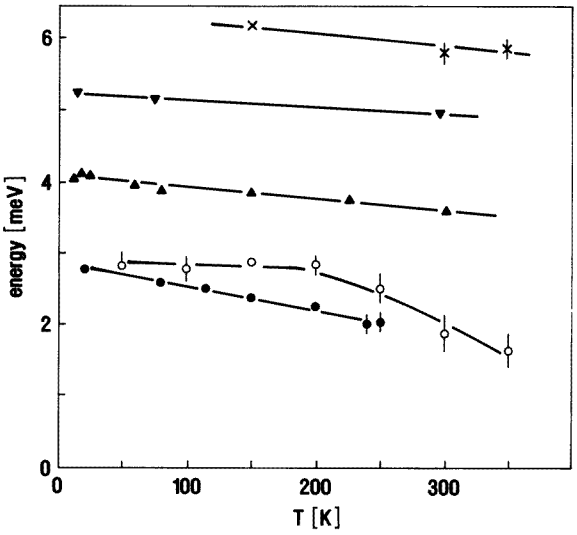

Figure 23. Librational frequencies as observed on powder samples of several fullerene compounds. Crosses: Rb_6C_{60} (Christides *et al* 1992); triangles pointing downwards: Rb_3C_{60} (Schober *et al* 1994); triangles pointing upwards: K_3C_{60} (Christides *et al* 1992); open circles: $RbNa_2C_{60}$ (Christides *et al* 1993); full circles: pure C_{60} (Neumann *et al* 1992b).

6.2. The internal vibrations of doped C_{60}

As intercalation of C_{60} with metal atoms entails only minor changes of the C_{60} molecule itself it had to be expected that the internal vibrations of doped C_{60} are not markedly different from those of the parent compound. The very first investigations confirmed this expectation (Prassides *et al* 1991). So the attention focused on subtle differences which might be associated with the insulator-to-metal-to-insulator transitions induced by increasing doping levels.

In a metal, electron–phonon coupling produces both a broadening and a softening of the affected phonon modes. Quantitatively such effects may be estimated using the expressions (Prassides *et al* 1993):

$$\Delta\omega \approx -(\lambda_v/5)\omega_v \tag{5}$$

and

$$\Gamma_v \approx (\Pi/5)N(E_F)\lambda_v\omega_v^2 \tag{6}$$

where $\Delta\omega_v$ is the change in frequency, Γ_v is the increase in full-width at half maximum, λ_v is the electron–phonon coupling constant for the vth phonon and $N(E_F)$ is the electron density of states at the Fermi energy. Provided that all the λ_v can be determined experimentally the superconducting transition temperature T_c can be calculated approximately from a relation

$$T_c \approx \bar{h}\omega_p \exp(-1/\lambda) \tag{7}$$

where ω_p is an average phonon frequency and λ the sum of the individual λ_vs. We note that, in general, the λ_v depend also on the phonon wavevector $\boldsymbol{q}$ so that a calculation of λ also implies an averaging over the whole Brillouin zone. In the case of doped C_{60}, however, it is reasonable to assume that the electron–phonon coupling strength will vary very little with $\boldsymbol{q}$ as doped C_{60} is a molecular solid. Therefore, a determination of the λ_vs can be based on a measurement of the phonon density of states (PDOS).

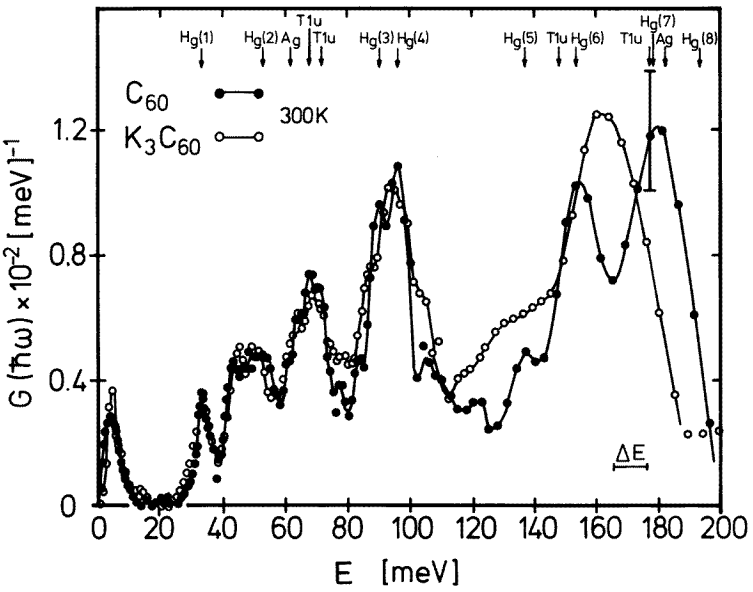

Figure 24. Comparison of the vibrational density of states as measured by Gompf *et al* (1994) for pure C_{60} and K_3C_{60}. The measurement was performed with a low incident energy in the neutron energy gain mode which leads to a very low scattered intensity for energy transfers exceeding ~100 meV. As a consequence, the error bars are rather large in this energy range. The frequencies of the Raman active modes of pure C_{60} as measured by Eklund *et al* (1992) are indicated by arrows. (Reprinted from Gompf F *et al* 1994 *J. Superconductivity* **7** 643, figure 3. Courtesy of Plenum Publishing Corporation.)

Measurements were performed (i) on reactor-based (Gompf *et al* 1994) and (ii) on spallation source-based instruments (Prassides *et al* 1991b, Prassides *et al* 1992, White *et al* 1992). The spectra obtained on these two types of instruments can be characterized by, roughly speaking, good counting statistics and poor resolution (case (i)), or poor counting statistics and good resolution (case (ii)). Examples of spectra are depicted in figures 24 and 25. The spectra show a general trend to lower phonon frequencies with increasing doping level by a few %. In particular, the high-energy cut-off in the PDOS softens from 205 meV (C_{60}) through 198 meV (C_{60}^{3-}) to 190 meV (C_{60}^{6-}) (Prassides *et al* 1992). The slight softening when going from C_{60} to C_{60}^{3-} was reproduced by an *ab initio* investigation of the vibrational and geometrical properties of solid C_{60} and K_3C_{60} (Bohnen *et al* 1995). It is tempting to associate the phonon softening observed on going from insulating C_{60} to superconducting M_3C_{60} with electron–phonon coupling induced effects described by relation (5), but part of the softening may well be related to slight changes in the molecular structure which makes an evaluation of λ_ν via (5) ambiguous. The observation that there is a further phonon softening when going from superconducting M_3C_{60} to insulating M_6C_{60} is a clear warning signal to interpret frequency changes between C_{60} and M_3C_{60} on the basis of (5).

On the other hand, changes in the phonon linewidth should indeed be related to differences in the electron–phonon coupling strength. The most pronounced effect was found for the $H_g^{(2)}$ mode at $E = 58$ meV, which strongly broadens when going from C_{60} to K_3C_{60} but is narrow again in Rb_6C_{60} (Prassides *et al* 1992). The electron–phonon coupling constant for this mode in K_3C_{60} evaluated from the data via (6) is about 30% of the total λ

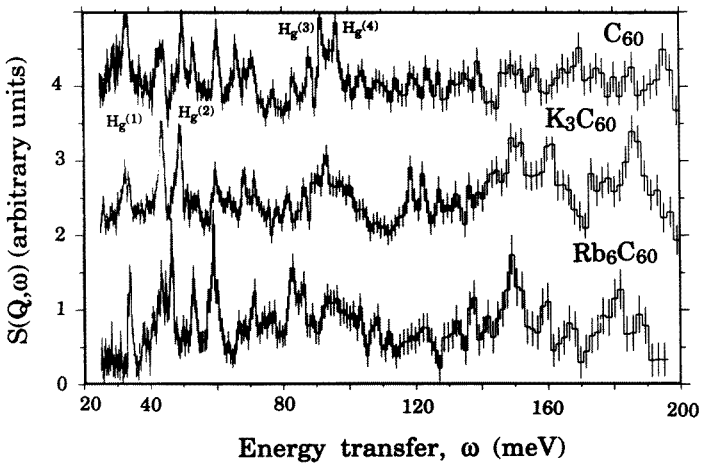

Figure 25. Inelastic neutron scattering spectra of the intramolecular modes of C_{60} (20 K), K_3C_{60} (5 K) and Rb_6C_{60} (20 K). (Reprinted from Prassides K *et al* 1992 *Carbon* **30** 1277, figure 6. Courtesy of Pergamon Press.)

needed to explain T_c via (7). The missing part of λ is probably contributed by many other modes showing much smaller linewidths which are difficult to evaluate from the current data. So all that can be concluded from the available data is that the experimental results support the idea of a strong electron–phonon coupling in M_3C_{60} but better data are needed to extract λ with sufficient accuracy.

Finally, we want to point out that attempts to determine λ_v via (6) have also been made by Raman scattering techniques. Raman scattering offers a better resolution but is restricted to modes of H_g and A_g symmetry. The latter may not be a severe disadvantage as theory predicts that these modes have much larger λ_vs than the other ones. However, Raman scattering experiments have given conflicting results which is possibly related to the surface sensitivity of this technique. Neutron scattering experiments probe bulk properties and this may be the reason that the results reported by different groups are in relatively good agreement with each other. The neutron results clearly rule out some interpretations of Raman results, e.g. the extremely strong softening and broadening of $H_g^{(1)}$ modes in M_3C_{60} as reported by Winter and Kuzmany (1995).

6.3. Search for superconductivity-induced effects

When a sample is cooled below the superconducting transitions temperature T_c phonon frequencies and phonon linewidths may change as a result of the opening of the gap Δ in the electronic spectrum. Theory predicts that these effects are significant only for phonon energies $\hbar\omega \approx 2\Delta$. Even here the changes are in general quite small, i.e. a few per cent of the phonon energy or even less.

For A_3C_{60} the superconducting energy gap 2Δ is very small with respect to the maximum phonon energy (K_3C_{60}: $\approx$5.5 meV, Rb_3C_{60}: $\approx$8 meV), so that a search for superconductivity-induced effects is promising only for the external vibrations. Nevertheless, such a search was also undertaken for the internal vibrations in Rb_3C_{60} (White *et al* 1992). The authors of this study present their results as evidence of very strong changes at the high end of the spectrum, but frankly speaking, the results are totally inconclusive

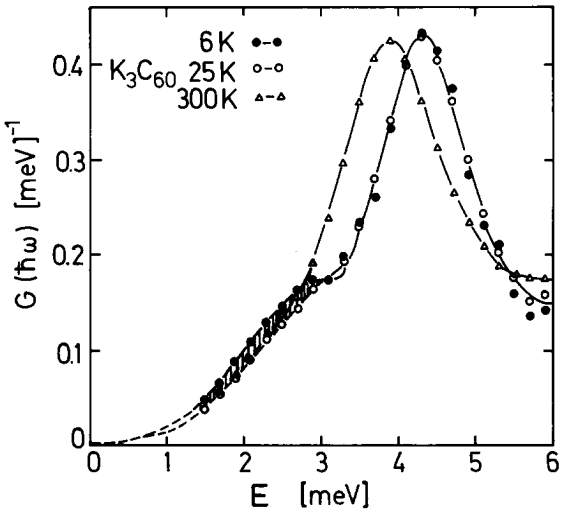

Figure 26. Temperature dependence of the spectrum of the intermolecular vibrations of K_3C_{60}. The softening of the lattice below T_c is indicated by the hatched area. (Reprinted from Gompf F *et al* 1994 *J. Superconductivity* **7** 643, figure 3. Courtesy of Plenum Publishing Corporation.)

because of very poor counting statistics.

In contrast, a softening of low-energy vibrations in K_3C_{60} and Rb_3C_{60} on cooling below T_c as reported by Renker *et al* (1993b) and Schober *et al* (1994) seems to be well established (see figure 26). However, at present it remains unclear whether this softening is really superconductivity-induced or only reflects a general trend not restricted to $T < T_c$ (Schober *et al* 1994). If the latter is true, the softening remains anomalous as phonon frequencies generally harden on cooling, but is most likely not associated with the onset of superconductivity. A confirmation of superconductivity-induced changes in the spectrum of the intermolecular modes would support theoretical results of Pickett *et al* (1994) who claim that the intermolecular modes of A_3C_{60} should contribute significantly to the total electron–phonon coupling constant.

7. Vibrations in solid C_{70}

7.1. Internal vibrations: differences to C_{60}

The internal vibrations of solid C_{70} have been studied by Christides *et al* (1993). The results are displayed in figure 27. When the spectrum of C_{70} is compared to that of C_{60} it appears that the low-energy cut-off is shifted to considerably lower frequencies (C_{60}: 35 meV; C_{70}: 28 meV), whereas the high energy cut-off remains practically unchanged. This finding can be understood in the following way: the low energy vibrations are deformation modes. The larger the molecule and the more it deviates from a spherical shape the less energy will be needed to deform the molecule by radial displacements of the atoms. As a consequence there will be some collective excitations of relatively low energy. On the other hand, the high-energy vibrations are bond-stretching modes, and as there is little difference between the average bond length in C_{60} and C_{70} there will be little difference between the frequencies of the bond-stretching vibrations of these two fullerenes.

Christides *et al* (1993) also gave results of a semiempirical calculation of the C_{70} vibrations using a quantum chemical force field method for II-electrons. The results of this method are not as accurate as those of the *ab initio* methods used for C_{60} but appear to be satisfactory. Later, Onida *et al* (1994) published results for C_{70} obtained by an *ab initio*

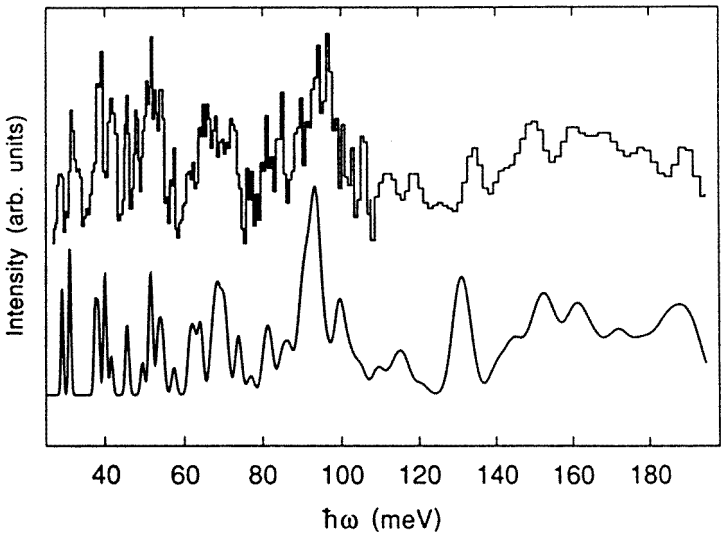

Figure 27. Upper curve: inelastic neutron scattering spectrum of solid C_{70} at $T = 20$ K. The spectrum was smoothed for $\hbar\omega > 110$ meV (Christides *et al* 1993). Lower curve: vibrational spectrum as calculated on the basis of an *ab initio* theory and convoluted with the instrumental resolution. (Reprinted from Onida G *et al* 1994 *Chem. Phys. Lett.* **219** 1, figure 1. Courtesy of Elsevier Science.)

method, which are in very good agreement with the experimental data (see the lower curve in figure 27). This good agreement is even more remarkable than that obtained for C_{60}, as the low symmetry of the C_{70} molecule greatly enhances the computational complexity.

7.2. External vibrations and their relationship to the structural phase transformations

The external vibrations of C_{70} have been investigated by means of inelastic neutron scattering by Renker *et al* (1993a) and Christides *et al* (1994). The first study covered the temperature range 200 K $\leqslant T \leqslant$ 320 K, whereas the temperature range investigated in the second study was considerably larger, i.e. 100 K $\leqslant T \leqslant$ 640 K. There is quite good agreement between the experimental results of the two groups.

In the ordered phase below $T \simeq 280$ K a peak was observed in the vibrational spectrum of C_{70} at energies $\hbar\omega \approx 2$ meV which is assigned to librational excitations (see figure 28). The energy of these librations is about 20% lower than that of the corresponding librations in the low temperature phase of C_{60} which shows that the rotational potential in solid C_{70} is rather soft. However, this softness applies presumably only to rotations around the long axis of the C_{70} molecules, whereas the potential for rotations around the short axis might be much stiffer. From a decomposition of the frequency distribution of the external vibrations into a translational and a librational part, Renker *et al* (1993) conclude that the librational part extends to an energy as high as ≈ 5 meV.

On approaching the order–disorder phase transition at $T \approx 280$ K from below little softening of the low-energy librations was observed in agreement with the fact that the phase transition is of first order. In the disordered phase a strong quasi-elastic signal was observed (see figure 28) indicative of a fast rotational diffusion of C_{70} molecules. Now the question arises: is the rotational diffusion isotropic or uniaxial? From the elongated shape of the C_{70} molecule (figure 1(*b*)) it is reasonable to assume that the rotational diffusion is

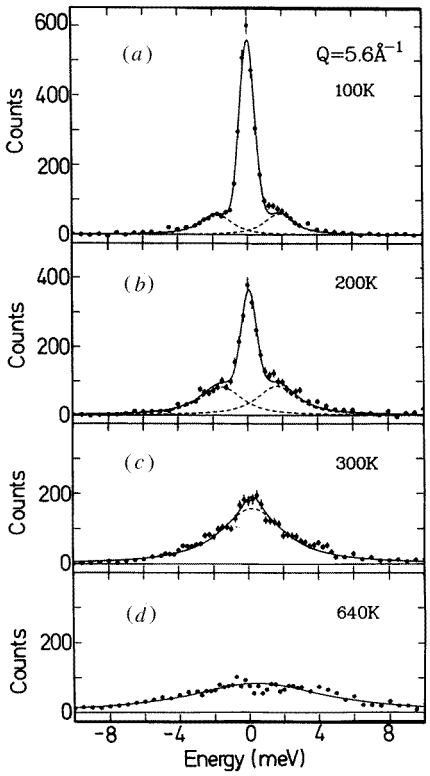

Figure 28. Neutron-inelastic-scattering spectra for polycrystalline C_{70} taken at $Q = 5.6$ Å^{-1} at different temperatures. The full curves are fitted curves and the broken curves show individual Lorentzian components of the fits. (Reprinted from Christides C *et al* 1994 *Phys. Rev.* B **49** 2897, figure 3 (redrawn). Courtesy of the American Institute of Physics.)

uniaxial rather than isotropic. This idea is supported by the single-crystal X-ray diffraction study of Blanc *et al* (1994). The two inelastic neutron scattering studies mentioned above both address this question but come to different conclusions: whereas Renker *et al* (1993a) argue that their data are slighly better described by a uniaxial rotational diffusion model, Christides *et al* (1994) favour an isotropic rotational diffusion model. This discrepancy is easy to understand by the fact that both models yield very similar predictions for the Q dependencies of the quasi-elastic scattering intensity and quasi-elastic linewidth after proper rescaling of the diffusion constant (figure 29). Therefore, it is extremely difficult to distinguish experimentally between the two models.

No qualitative change of the quasi-elastic signal has been observed by Christides *et al* (1994) on heating the sample above the next structural phase transformation at $T \approx 360$ K. It is generally believed that in the high temperature phase the reorientational motions of the C_{70} molecules are practically isotropic, and so it is not surprising that the neutron data could be well described by an isotropic rotational diffusion model. The diffusion constant at $T = 525$ K was found to be 50% higher than at $T = 300$ K when using the same model in both cases, i.e. $D_r = 1.5 \times 10^{10}$ s^{-1} and $D_r = 10 \times 10^{10}$ s^{-1}, respectively (see figure 28). When the same model was applied to C_{60} data taken at $T = 520$ K, a much larger diffusion constant was obtained ($D_r = 2.8 \times 10^{10}$ s^{-1}), which is easily understandable from the different shapes of the C_{60} and the C_{70} molecules.

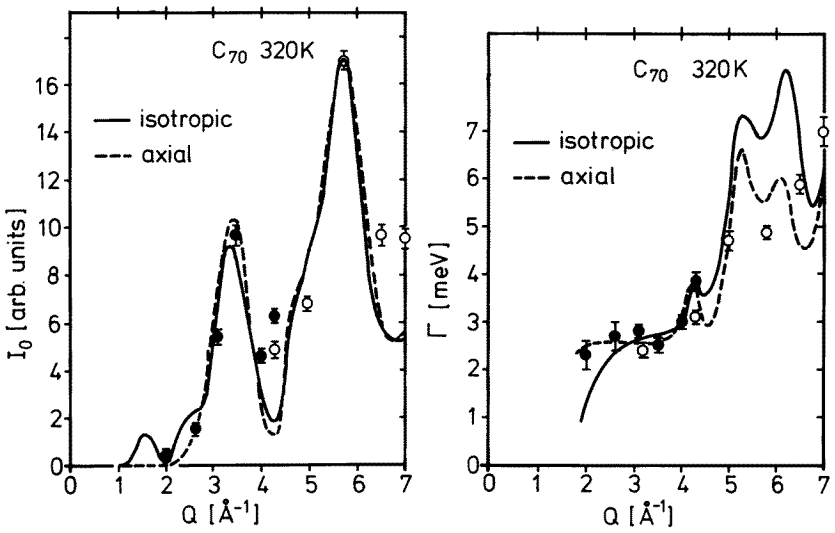

Figure 29. Q-dependence of the quasi-elastic integrated intensity (left) and of the quasi-elastic linewidth for C_{70} at $T = 320$ K. The full and broken curves were calculated from a model for isotropic and axial rotational diffusion, respectively. The theoretical results for the intensity were normalized to the measured value at $Q = 5.7$ Å^{-1}. The theoretical curves for the linewidth were obtained for a rotational diffusion constant $D_R = 1.6 \times 10^{10}$ s^{-1} (isotropic) and $D_R = 6.8 \times 10^{10}$ s^{-1} (axial), respectively. (Reprinted from Renker B *et al* 1993 *Z. Phys.* B **90** 325, figures 2(*b*) and 3(*b*). Courtesy of Springer-Verlag.)

8. Vibrations in fullerene derivatives

Out of the many fullerene derivatives synthesized so far only two have been investigated by inelastic neutron scattering, i.e. $C_{60}O$ (also called 6, 6 epoxide) and $C_{61}H_2$ (also called 5, 6 annulene). In $C_{60}O$ the oxygen bridges a bond between two hexagons, whereas in 5,6 annulene the CH_2 group bridges a bond between a hexagon and a pentagon (we note that there is another modification of $C_{61}H_2$ called 6, 6-cyclopropane, where the CH_2 group bridges a bond between two hexagons, but this modification has as yet not been investigated by inelastic neutron scattering).

The two C_{60} derivatives just mentioned undergo an order–disorder transition similar to the one found in pure C_{60}, i.e. from fcc (high-T) to simple cubic (low-T) (Vaughan *et al* 1992, Lommen *et al* 1994). The phase transitions are observed at slightly higher temperatures than in pure C_{60}, i.e. $T_s = 270$–280 K for $C_{60}O$ and $T_s \approx 290$ K for $C_{61}H_2$ annulene. The adducts occupy the octahedral and tetrahedral voids in both phases. In the low-temperature phase the intermolecular contacts are arranged in the same manner as in pure C_{60}, i.e. double bonds of one molecule face pentagons or hexagons of adjacent molecules. This means that the O or CH_2 appendage has only a minor effect on the solid state phase sequence.

The low-energy dynamics of $C_{60}O$ and $C_{61}H_2$ is also very similar to that of pure C_{60}: below the transition, a peak is observed in the neutron spectrum which corresponds to molecular librations, while above the transition the peak collapses into a quasi-elastic line characteristic of rotational diffusion (Pinschovius *et al* 1995d, Neumann *et al* 1995). The experimental results for $C_{60}O$ are depicted in figure 30. The peaks observed below the transition are relatively broad which indicates a broad range of librational frequencies. The

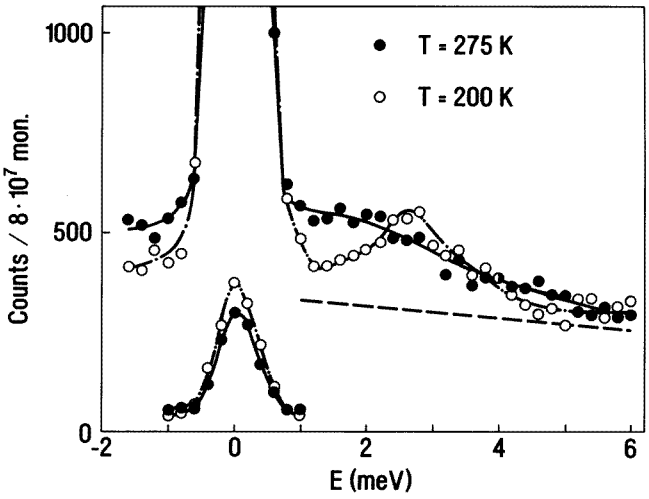

Figure 30. Inelastic-neutron-scattering spectra for the high and the low temperature phase of $C_{60}O$. Note the increase of the scattering intensity at $E = 0$ on cooling to $T = 200$ K which signifies that a considerable amount of static disorder is frozen in at the lock-in phase transition at $T = 270$ K. Curves are a guide to the eye. The broken curve is an estimate of the background (Pintschovius *et al* 1995d). (Reprinted from unpublished results of the author.)

occurrence of rather soft librations can be understood as an effect of the slighly expanded lattice constant when compared to pure C_{60}. The occurrence of rather stiff librations is probably due to the steric hindrance produced by the adducts. The steric hindrance is probably also the reason that the maxima in the librational spectra of $C_{61}H_2$ and $C_{60}O$ is shifted to slightly higher energies when compared to pure C_{60}: at $T = 200$ K the maxima are observed at $E = 2.2$ meV, 2.5 meV and 2.7 meV for C_{60}, $C_{61}H_2$ and $C_{60}O$, respectively.

9. Concluding remarks

Neutron studies of fullerenes have provided a wealth of information on the binding properties of these compounds. A comparison of the experimental results with predictions from *ab initio* theory can be briefly summarized by very good understanding of the strong intramolecular forces and poor understanding of the weak intermolecular forces. Why is the situation so different for the weak and the strong forces? One reason is that a much larger computational effort is needed to investigate not only the intramolecular but also the intermolecular forces: whereas an investigation of the intramolecular forces can be based on calculations for isolated molecules, an investigation of the intermolecular forces requires calculations for realistic crystallographic structures with four molecules in the unit cell, which is barely feasible with present-day computers. With further progress in computer speed such calculations will become feasible some years ahead. However, faster computers may not be enough to solve the problem: present-day *ab initio* theories of the electronic properties use approximations (the so-called local-density approximation) which seem to work very well only for regions of high electron density, but not for the regions of the rather low electron density of the weak intermolecular bonds.

The weak intermolecular bonds are usually explained by vdW forces. As there is a theoretical basis for the r^{-6} dependence of vdW forces it is generally believed that we

have understood this type of bonding. However, the prefactor of the potential cannot be calculated from first principles, and the large scatter of empirically determined prefactors indicates that empirical 'vdW' potentials include contributions to the chemical bonding which are not really vdW-like. The unexpectedly stiff orientational potential in solid C_{60} clearly shows that the weak intermolecular forces cannot be adequately understood as vdW forces, so that further progress in theory on this matter is highly desirable.

Acknowledgments

The author is indebted to Dr W Reichardt and Dr R Heid for carefully reading the manuscript.

References

Adams G B, Page J B, Sankey O F, Sinha K, Menendez V and Huffmann D R 1991 *Phys. Rev.* B **44** 4052–5
Andreoni W 1993 *The Physics and Chemistry of the Fullerenes (NATO-ASI Series C 443)* ed K Prassides pp 169–82
Axe J D, Moss S C and Neumann D A 1994 *Solid State Physics* vol 48 ed H Ehrenreich and F Spaepen (New York: Academic) pp 149–224
Bethune D S, Meijer G, Tang W L, Rosen H J, Golden W G, Seki H, Brown C A and deVries M S 1991 *Chem. Phys. Lett.* **179** 181–4
Blanc E, Bürgi H-B, Restori R, Schwarzenbach D, Stellberg P and Venugopalau P 1994 *Europhys. Lett.* **27** 359–64
Blaschko O, Glas R, Maier C, Haluska M and Kuzmany H 1993 *Phys. Rev.* B **48** 14638–41
Bohnen K P, Heid R, Ho K M and Chan C T 1995 *Phys. Rev.* B **51** 5805–13
Bürgi H-B, Blanc E, Schwarzenbach D, Liu S, Lu Y, Kappes M M and Ibers J 1992 *Angew. Chem. Int. Ed. Engl.* **31** 640–2
Burgos E, Halac E and Bonaedo M 1993 *Phys. Rev.* B **47** 7542–5
Cappelletti R L, Copley J R D, Kamitakahara W A, Li F, Lannin J S and Ramage D 1991 *Phys. Rev. Lett.* **66** 3261–4
Chaplot S L and Pintschovius L 1995a *Full. Sci. Technol.* at press
Chaplot S L, Pintschovius L, Haluska M and Kuzmany H 1995b *Phys. Rev.* B **51** 17028–34
Chow P C, Jiang X, Reiter G, Wochner P, Moss S C, Axe J D, Hanson J D, McMullan R K, Meng R L and Chu C W 1992 *Phys. Rev. Lett.* **69** 2943–6
Christides C, Dennis T J S, Prassides K, Cappelletti R L, Neumann D A and Copley J R D 1994 *Phys. Rev.* B **49** 2897–903
Christides C, Neumann D A, Prassides K, Copley J R D, Rush J J, Rosseinsky M J, Murphy D W and Maddon R C 1992 *Phys. Rev.* B **46** 12 088–91
Christides C, Nikolaev A V, Dennis R J S, Prassides K, Negri F, Orlandi G and Zerbetto F 1993 *J. Phys. Chem.* **97** 3641–3
Copley J R D, Neumann D A, Cappelletti R L and Kamitakahara W A 1992 *J. Phys. Chem. Solid* **53** 1353–71
Copley J R D, Neumann D A and Kamitakahara W A 1995 *Can. J. Phys.* at press
Coulombeau C, Jobic M, Bernier P, Fabre C, Schutz D and Rassat A 1992 *J. Phys. Chem.* **96** 22–4
Coulombeau C, Jobic H, Carlile C J, Bennington S M, Fabre C and Rassat A 1994 *Full. Sci. Technol.* **2** 247–54
David W I F, Ibberson R M, Dennis T J S, Hare J P and Prassides K 1992 *Europhys. Lett.* **18** 219–24; an addendum appeared in 1992 *Europhys. Lett.* **18** 735–6
David W I F, Ibberson R M and Matsuo T 1993 *Proc. R. Soc.* A **442** 129–46
Eklund P C, Zhou P, Wang K A, Dresselhaus G and Dresselhaus M S 1992 *J. Phys. Chem. Solid* **53** 1391
Faulhaber J C R, Ko D Y K and Briddon P R 1993 *Phys. Rev.* B **48** 661–4
Feuston B P, Andreoni W, Parinello M and Clementi E 1991 *Phys. Rev.* B **44** 4056–9
Gompf F, Renker B, Schober H, Adelmann P and Heid R 1994 *J. Supercond.* **7** 643–5
Gunnarsson O, Satpathy S, Jepsen O and Andersen O K 1991 *Phys. Lett.* **67** 3002–5
Guo Y, Karasawa N and Goddard III W A 1991 *Nature* **351** 464–7
Hebard A F, Rosseinsky M J, Haddon R C, Murphy D W, Glarum S H, Palstra T T M, Ramirez A P and Kortan A R 1991 *Nature* **350** 600–1
Hedberg K, Hedberg L, Bethune D S, Brown C A, Dorn M C, Johnson R D and de Vries M 1991 *Science* **254** 410–2
Heid R, Pintschovius L, Reichardt W, Launois P and Moret R 1995 unpublished results

Heiney P A, Fischer J E, McGhie A R, Romanow W J, Denenstein A M, McCauley Jr J P, Smith III A B and Cox D E 1991 *Phys. Rev. Lett.* **67** 1467–70
Heiney P A *et al* 1992 *Phys. Rev.* B **45** 4544–7
Jishi R A, Mirie R M and Dresselhaus M S 1992 *Phys. Rev.* B **45** 13 685–9
Jones R, Lutham C D, Heggie M I, Torres V J B, Oberg S and Estreicher S K 1992 *Phil. Mag. Lett.* **65** 291–8
Krätschmer W, Lamb L D, Fostiropoulos K and HuSmann D R 1990 *Nature* **347** 354–8
Kroto H W, Heath J R, O'Brian S C, Curl R F and Smalley R E 1985 *Nature* **318** 162–3
Leclereq F, Damay P, Foukani M, Chieux P, Bellissent-Funel M C, Rassat A and Fabre C 1993 *Phys. Rev.* B **48** 2748–58
Liu S, Lu Y, Kappes M M and Ibers J A 1991 *Science* **254** 408–10
Lommen A N *et al* 1994 *Phys. Rev.* B **49** 12572
Lu J, Li X and Martin R M 1992 *Phys. Rev. Lett.* **68** 1551–4
Meingast C and Gugenberger F 1993 *Mod. Phys. Lett.* B **7** 1703–24
Meingast C, Gugenberger F, Roth G, Haluska M and Kuzmany H 1994 *Z. Phys.* B **95** 67–71
Neumann D A *et al* 1992a *Phys. Rev. Lett.* **67** 3808–11
——1992b *J. Chem. Phys.* **96** 8631–3
Neumann D A, Fischer J E, Copley J R D, Rush J J, McGhie R M, Strongin R M and Smith III A B 1995 *Lecture given at the APS meeting 24*
Onida G, Andreoni W, Kohanoff J and Parrinello M 1994 *Chem. Phys. Lett.* **219** 1–7
Onida G and Benedek G 1992 *Europhys. Lett.* **18** 403–8
Pickett W E, Papaconstantopoulos D A, Pederson M R and Erwin S C 1994 *J. Supercond.* **7** 651–5
Pintschovius L 1994 *Nucl. Instrum. Methods* A 338 136–143
Pintschovius L and Chaplot S L 1995a *Z. Phys.* B **98** 527–40
Pintschovius L, Chaplot S L, Heid R, Haluska M and Kuzmany H 1993 *Electronic Properties of Fullerenes (Springer Series in Solid State Sciences 117*) ed H Kuzmany, J Fink, M Mehring and S Roth (Berlin: Springer) pp 162–7
Pintschovius L, Chaplot S L, Roth G, Haluska M and Kuzmany H 1995b *Phys. Scr.* T **57** 102–6
Pintschovius L, Chaplot S L, Roth G and Heger G 1995c *Phys. Rev. Lett.* **75** 2843–6
Pintschovius L, Kappes M M, Michel R H and Stoermer C 1995d to be published
Pintschovius L, Renker B, Gompf F, Heid R, Chaplot S L, Haluska M and Kuzmany H 1992 *Phys. Rev. Lett.* **69** 2662–5
Prassides K, Dennis T J S, Hare J P, Tomkinson J, Kroto H W, Taylor R and Walton D R M 1991a *Chem. Phys. Lett.* **187** 455–8
Prassides K, Christides C, Rosseinsky M J, Tomkinson J, Murphy D W and Haddon R C 1992 *Europhys. Lett.* **19** 629–36
Prassides K, Kroto H W, Taylor R, Walton D R M, David W I F, Tomkinson J, Haddon R C, Rosseinsky M J and Murphy D W 1993 *The Fullerenes* ed H W Kroto, J E Fischer and D E Cox (Oxford: Pergamon) 139–48
Prassides K, Tomkinson J, Christides C, Rosseinsky M J, Murphy D W and Haddon R C 1991b *Nature* **354** 462–3
Renker B, Gompf F, Heid R, Adelmann P, Heiming A, Reichardt W, Roth G, Schober H and Rietschel H 1993a *Z. Phys.* B **90** 325–9
Renker B, Gompf F, Schober H, Adelmann P, Bornemann H J and Heid R 1993b *Z. Phys.* B **92** 451–5
Reznik D, Kamitakahara W A, Neumann D A, Copley J R D, Fischer J E, Strongin R M, Cichy M A and Smith III A B 1994 *Phys. Rev.* B **49** 1005–10
Rosseinsky M J 1994 *The Physics and Chemistry of the Fullerenes (NATO-ASI Series C 443)* ed K Prassides pp 245–62
Rosseinsky M J, Ramirez A P, Glaram S H, Murphy D W, Haddon R C, Hebard A F, Palstra T T M, Kortan A R, Zahurak S M and Makkija A V 1991 *Phys. Rev. Lett.* **66** 2830–3
Roth G and Adelmann P 1992 *J. Physique I* **2** 1541–8
Schiebel P, Wulf K, Prandl W, Meyer G, Papoular R and Paulus W 1995 *Acta Cryst.* at press
Schober H, Renker B, Gompf F and Adelmann P 1994 *Physica* **235–40C** 2487–8
Skalyo Jr J, Endoh Y and Shirane G 1974 *Phys. Rev.* B **9** 5300
Sprik M, Cheng M and Klein M L 1992 *J. Phys. Chem.* **96** 2027–30
Stanton R E and Newton M D 1988 *J. Phys. Chem.* **92** 2141
Tycko R, Dabbagh G, Fleming R M, Haddon R C, Makhija A V and Zahurak S M 1991 *Phys. Rev. Lett.* **67** 1886–9
Van Tendeloo G, Amelinckx S, DeBoer J L, Smaalen van S, Verheijen M A, Meekes H and Meijer G 1993 *Europhys. Lett.* 329–34
Vaughan G B M *et al* 1992 *Chem. Phys.* **168** 185
Wang C Z, Xu C M, Chan C T and Ho K M 1991 quoted in Cappelletti *et al* 1991 Private communication

Wang X Q, Wang C Z and Ho K M 1993 *Phys. Rev.* B **48** 1884–7
White J W, Lindsell G, Pang L, Palmisano A, Silvia D S and Tomkinson J 1992 *Chem. Phys. Lett.* **191** 92–6
Winter J and Kuzmany H 1995 *Proc. Internat. Winterschool on Electronic Properties of Novel Materials (Kirchberg/Tirol)* (Singapore: World Scientific) 4.3–11.3.95 to appear
Yildirim T, Harris A B, Erwin S C and Pederson M R 1993 *Phys. Rev.* B **48** 1888–98
Yu J, Kalia R K and Vashishta P 1993 *Appl. Phys. Lett.* **63** 3152–4
Zhou O and Cox D 1993 *The Fullerenes* ed H W Kroto, J E Fischer and D E Cox (Oxford: Pergamon) pp 203–20
Zhou O, Fischer J E, Coustel N, Kycia S, Zhu Q, McGhie A R, Romanow W R, McCauley Jr J P, Smith III A B and Cox D E 1991 *Nature* **351** 462–4